NOAA Atlas 15 Pilot Technical Report

NOAA Office of Water Prediction

March 25, 2025

Version 1.1.p

DISCLAIMER

The data and information presented in this report are provided to demonstrate current progress on the various tasks associated with this project. Values presented herein are preliminary and intended for comparison and feedback purposes only as this analysis has not completed the peer review process as is standard with NOAA precipitation frequency studies.

Acknowledgements

This document was carefully prepared by NOAA Atlas 15 technical team members:

- Sanja Perica, IBSS Corporation (RTI)
- Janel Hanrahan, RTI International (RTI)
- Marcelo Lago, LAGO Consulting & Services (LAGO)
- Ken Kunkel, North Carolina State University (NCSU)
- Debbie Martin, RTI International (RTI)

And reviewed by:

- Sandra Pavlovic, NOAA/NWS Office of Water Prediction
- Greg Fall, NOAA/NWS Office of Water Prediction
- Fernando Salas, NOAA/NWS Office of Water Prediction
- Fred Ogden, Chief Scientist, NOAA/NWS Office of Water Prediction

Creation of the NOAA Atlas 15 Pilot datasets required the contributions and support of people and organizations across the government, private industry, and academia. The Office of Water Prediction extends thanks and appreciation to:

- All technical members of the NOAA Atlas 15 team (listed in alphabetical order): Idoliris Bacallao (LAGO), Brian Beitler (IBSS), Maria Bravo (LAGO), Ryan Clare (IBSS), Tori Clear (IBSS), Jacquelyn Crowell (IBSS), Josh Eston (RTI), Nestor Hernandez (LAGO), Sydney Lybrand (IBSS), Jennifer Lake Marchetti (IBSS), Bowen Pan (RTI), Cody Polera (IBSS), Kevin Sanchez (IBSS), Liqiang Sun (NCSU), Xia Sun (NCSU), Alana Shuvalau (IBSS), David Tedesco (IBSS), John Tenenholtz (LAGO), Lynne Trabachino (RTI), Danielle White (IBSS), and Shu Wu (RTI).
- All technical members of the NOAA Atlas 14 team (listed in alphabetical order): Austin Jordan (IBSS), Michael St. Laurent (RTI), Rama Sesha Sridhar Mantripragada (IBSS), Carl Trypaluk (RTI), and Dale Unruh (RTI).
- All subject matter experts who attended the NOAA Atlas 15 technical workshops for federal partners, hosted virtually on January 18, 2023, and August 14, 2024.
- Individuals and groups who provided feedback on the National Weather Service Public Notification Statement published on September 15, 2022.
- All subject matter experts and other members of the National Academies of Sciences, Engineering, and Medicine, committee on Modernizing Probable Maximum Precipitation Estimation.
- Subject matter experts who support the memorandum of understanding established between NOAA and both the American Society of Civil Engineers (ASCE), and the Federal Highway Administration (FHWA).
- The many other diligent individuals who impacted and contributed to this project with their expertise, guidance, and commitment, including David Conrad, Elizabeth Duffy, Meg Galloway (Association of State Floodplain Managers), John England (U.S. Army Corps of Engineers), Michelle Irizarry-Ortiz (United States Geological Survey), Joseph Krolak and Robert Kafalenos (Federal Highway Administration), and Kelly Mahoney (NOAA Oceanic and Atmospheric Research).

Please direct all questions to atlas15.info@noaa.gov.

Preferred citation for the Atlas 15 Pilot Technical Report:

Perica, S., J. Hanrahan, M. Lago, K. Kunkel, and D. Martin, 2025: Atlas 15 Pilot Technical Report Version 1.1.p. NOAA. National Weather Service, Office of Water Prediction, Silver Spring, MD.

Version history of NOAA Atlas 15 release dates and the nature of changes made are listed below:

Version	**Released Date**	**Notes**
Version 1.0.p	September 26, 2024	NOAA Atlas 15 Pilot data and documentation released for review.
Version 1.1.p	March 25, 2025	NOAA Atlas 15 Pilot documentation updated to reflect a terminology change.

Table of Contents

NOAA Atlas 15 Pilot Technical Report

1. Executive Summary

The Office of Water Prediction (OWP) of the National Oceanic and Atmospheric Administration's (NOAA) National Weather Service (NWS) is responsible for the development, production, and publication of precipitation frequency (PF) estimates for the United States and affiliated territories. These estimates require periodic updates to account for new data and improved methodologies. Since the early 2000s, OWP has updated PF estimates for various regions of the country and published them as Volumes in the NOAA Atlas 14 series (https://hdsc.nws.noaa.gov/pfds/). The analysis and methodologies used to estimate precipitation frequencies in the NOAA Atlas 14 series assumed that the climate is stationary in a statistical context.

In 2022, NOAA received federal funding under the Bipartisan Infrastructure Law to revise and update NOAA PF estimates nationwide to account for a changing climate. Once complete, updated national estimates will be published in two volumes of NOAA Atlas 15: Volume 1 will provide PF estimates that account for temporal trends in historical observations, and Volume 2 will provide PF estimates projected into the future under different carbon emissions scenarios based on climate model projections. NOAA Atlas 15 will provide seamless estimates for the contiguous United States (CONUS) and outside the contiguous United States (oCONUS) regions.

NOAA Atlas 15 begins with a prototype framework developed over the state of Montana, which serves as a pilot domain. The deliverables include precipitation frequency estimates and the corresponding upper and lower bounds of 90% confidence intervals for a subset of durations and frequencies. These estimates are provided as gridded datasets and interactive graphics queryable using a web interface that was developed for this purpose. Examples of PF estimates are provided for both the Volume 1 and Volume 2 data for the pilot domain, and are delivered alongside supporting documentation describing the underlying methods.

2. Introduction

The NOAA Atlas 15 methods described here expand upon a framework that was developed and summarized in the *Assessment Report: Analysis of Impact of Nonstationary Climate on NOAA Atlas 14 Estimates* (OWP, 2022). This framework arose from a multi-year assessment of the suitability of modern nonstationary precipitation frequency methodologies and an evaluation into the feasibility of using downscaled climate model data to extract future precipitation frequency estimates in the presence of a nonstationary climate regime. The resulting *Assessment Report* underwent broad review by stakeholders and federal partners.

Building upon NOAA Atlas 14 (referred to as Atlas 14 herein) and the *Assessment Report* recommendations, NOAA Atlas 15, Volume 1, applies historical precipitation observations to generate quality-controlled nonstationary precipitation frequency estimates that reflect observed trends. Furthermore, the methodology used to produce NOAA Atlas 15, Volume 2, will apply downscaled climate model projections to generate estimates for the future under different carbon emissions scenarios. The prototype framework for the NOAA Atlas 15 pilot presented here (referred to as Atlas 15 herein) encompasses methodologies for:

- Computation of precipitation frequency estimates at station locations using a nonstationary regional precipitation frequency analysis method;

- Spatial interpolation of precipitation frequency estimates to a high-resolution grid; and,
- Application of adjustment factors to account for future changes in the estimates.

For the purpose of producing preliminary results for public comment on the methodologies, initial testing of Volume 1 and Volume 2 was limited to the state of Montana (see Section 3). However, the proposed framework is intended to be applicable to the CONUS and oCONUS domains.

Appendix A contains a list of acronyms and abbreviations used throughout this document. Appendix B provides standard definitions.

3. NOAA Atlas 15 Pilot

3.1. Pilot Domain

Atlas 15 is initiated by the development of a pilot product over the state of Montana (Figure 1). This area was selected due to its diverse terrain characteristics, the availability of current quality-controlled data from the recently published Atlas 14 Volume 12, which includes the states of Idaho, Wyoming, and Montana, and the opportunity for side-by-side comparison with precipitation frequency estimates produced using the legacy stationary approach (e.g., Perica et al., 2018).

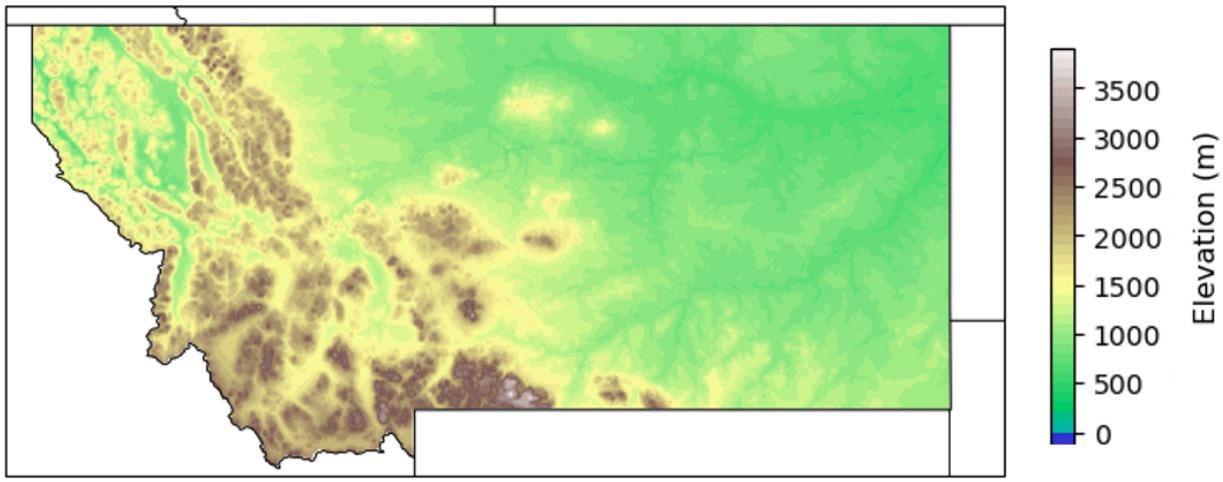

Figure 1. NOAA Atlas 15 pilot domain.

3.2. Pilot Overview

The Atlas 15 pilot includes precipitation frequency estimates over the state of Montana with upper and lower 90% confidence interval bounds on a 30-arc second geographic grid (approximately 0.9 km x 0.6 km at this latitude) for selected durations and annual exceedance probabilities (AEPs), as defined in Table 1. Volume 1 estimates, which represent conditions in 2023 as illustrated in Figure 2, were developed according to the nonstationary framework described in Section 4. Volume 2 estimates were developed by applying adjustment factors, obtained from downscaled climate model outputs, to Volume 1 estimates, as described in Section 5. These are available for future time periods within two distinct frameworks: global temperature index (GTI) and emissions scenario, which are illustrated in Figure 2. The GTI framework provides estimates at specified levels of model-average global temperature

anomalies relative to preindustrial values. These estimates are derived from the points in time at which models have warmed to each specified benchmark (1.5 - 5°C). In general, these points in time will differ from model to model. Unlike the GTI framework, the emissions scenario framework provides estimates at specified points in time, at the resolution of decades (2030 – 2100), under two different shared socioeconomic pathways (SSP2-4.5 and SSP5-8.5), further described in Section 5.1.3. These frameworks and their applications are discussed in more detail in Section 5.

Table 1. Atlas 15 pilot precipitation frequency estimates data availability.

	Volume 1	Volume 2	
Framework	**n/a**	**GTI**	**Scenario (SSP2-4.5 and SSP5-8.5)**
Range	2023	1 – 5°C	2030 – 2100
Durations	60-min, 2-hr, 3-hr, 6-hr, 12-hr, 24-hr, 2-day, 3-day, 4-day, 7-day, 10-day		
AEP*	50%, 20%, 10%, 4%, 2%, 1%		
Spatial resolution	30-arc second grid		

*Annual exceedance probability (AEP) is a probability associated with exceeding a given amount of precipitation at a given location for a specified duration at least once in any given year. The inverse of AEP provides a measure of the average time between years in which a value is exceeded at least once. For example, the AEP inverse of 2% corresponds to an average recurrence interval of 50 years.

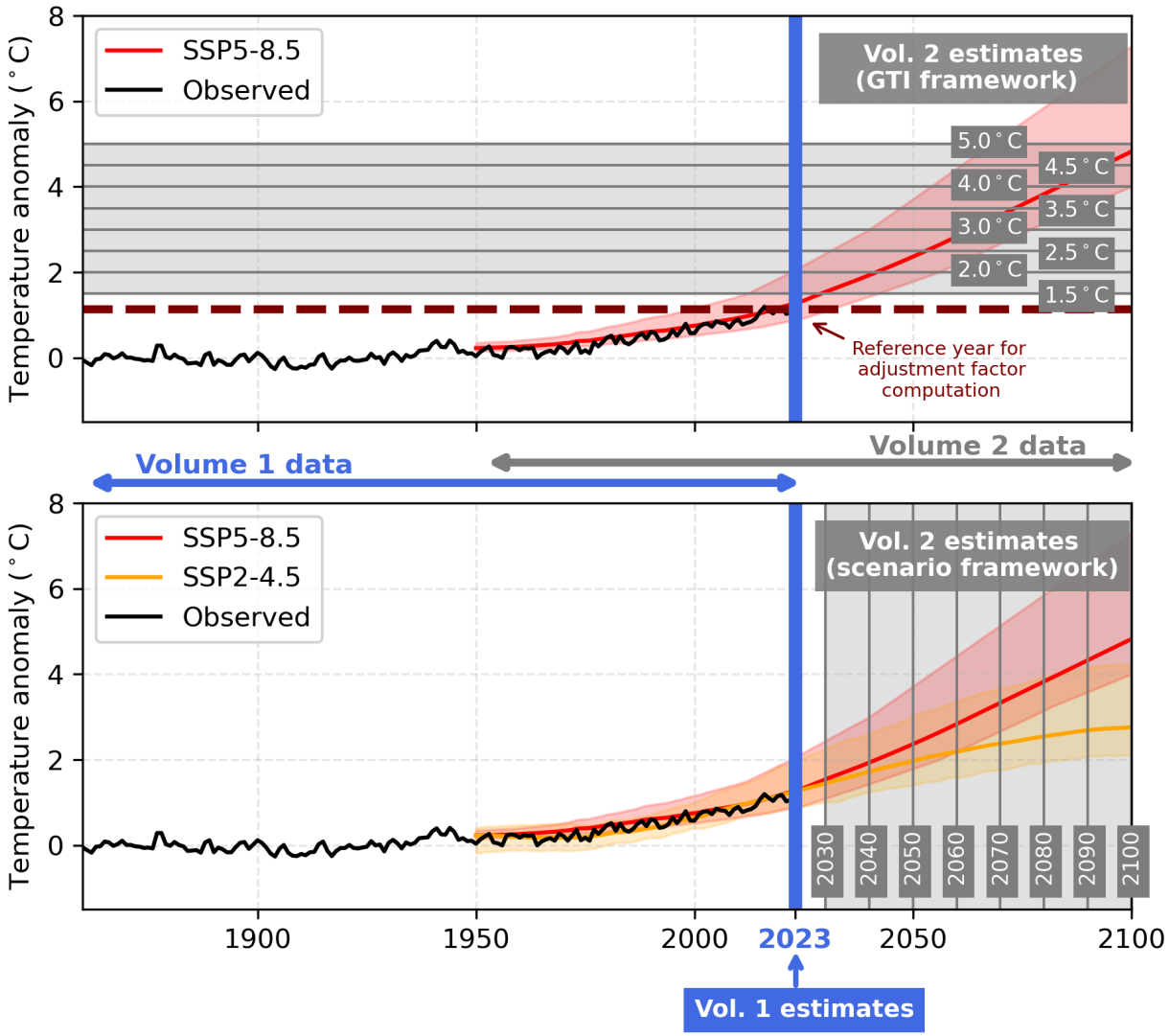

Figure 2. Availability of NOAA Atlas 15 pilot estimates. Volume 1 estimates were informed by historical observation data and are available for the current time (2023). Volume 2 adjustment factors were informed by model data and estimates are available for specific global temperature anomalies according to the GTI framework (top) and for future decades according to the scenario framework (bottom).

4. NOAA Atlas 15 Pilot Volume 1

4.1. Background and Overview

The methodology used to produce the PF estimates in Atlas 14 involved fitting the Generalized Extreme Value (GEV) distribution to quality-controlled unconstrained annual maximum series (AMS) data at individual stations using a regional approach. Distribution parameters, and the resulting precipitation frequency estimates at each station location, were determined based on the mean of the annual maximum series at the station and regionally derived higher order L-moments. Grids of precipitation frequency estimates for each duration were then generated based on mean annual maximum (MAM) grids and at-station precipitation frequency estimates for that duration (e.g., Perica et al., 2018).

For the Atlas 15 pilot framework, the GEV distribution fitting used a different method that used the regional Maximum Likelihood Estimation (MLE) parameterization approach, primarily

because of MLE's ability to incorporate temporal covariates (e.g., GTI) that can account for a non-stationary climate. Additionally, the MLE approach can include other spatial covariates (e.g., MAM, elevation) that may improve inference on the distribution of extreme precipitation.

Similar to Atlas 14, the Atlas 15 pilot framework uses a regional approach to produce precipitation frequency estimates at each station location by pooling AMS data from selected nearby stations. Regional delineations for both approaches are determined by evaluating geographical properties at station locations with respect to mountain ridges and elevation differences, in addition to differences in meteorological properties. While the Atlas 14 regional delineation decisions resulted from a combination of automatic and manual inspections, the process for the Atlas 15 is fully automated.

4.2. Relevant Datasets

Because Atlas 14 Volume 12 includes the pilot domain, Atlas 15 development took advantage of the QA/QC'd rain gauge and other data produced or acquired for the Atlas 14, Volume 12, project. Specifically, data obtained from the Atlas 14 effort included:

- Metadata for daily and sub-daily stations in Montana and an approximate 30-km buffer area (see Fig. 3);
- Quality controlled AMS precipitation data, defined as the highest precipitation amounts per year over 60-min, 6-hr, 24-hr, 4-day, and 10-day durations for those stations;
- Gridded mean annual maximum (MAM) precipitation and mean annual precipitation (MAP) data at 30-arc second resolution, originally obtained from the Oregon State University's PRISM (Parameter-Elevation Regressions on Independent Slopes Model) Group (Daly et al., 2002; Perica et al., 2018).

In addition, the following data were collected:

- Annual global near-surface temperature anomalies for 1850 - 2023 from NOAA's National Centers for Environmental Information (NCEI, 2023);
- NASA's 90-meter Shuttle Radar Topographic Mission (SRTM90) digital elevation model (DEM) grids (NASA, 2023).

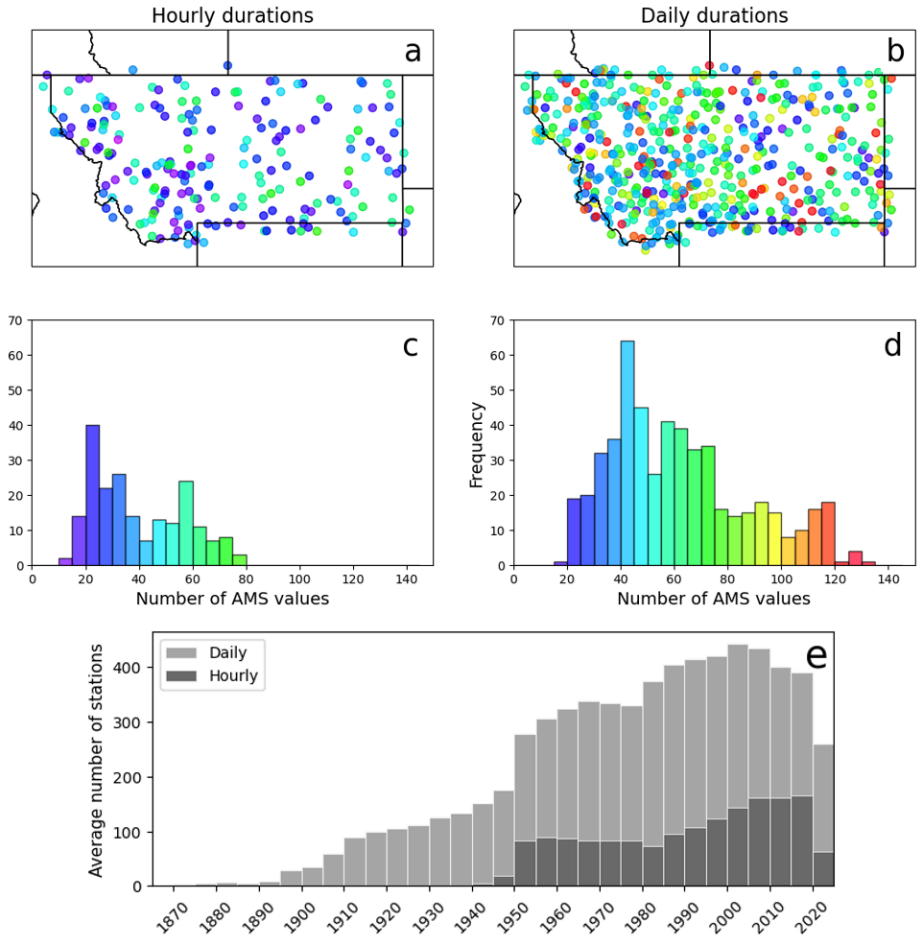

Figure 3. Station locations and histograms illustrating the number of AMS values per station for hourly (a,c) and daily (b,d) durations, and the number stations per year within this domain averaged over 5-year periods (e).

4.3. Methods

4.3.1. Statistical Distribution Fitting

For the Atlas 15 Volume 1 pilot framework, the regional Maximum Likelihood Estimation (MLE) approach was used to estimate the GEV distribution parameters at all station locations within the domain for selected durations identified in Table 1. The 4-parameter Kappa distribution was also tested as an alternative distribution based on feedback received during public review of the *Assessment Report* (OWP, 2022), but preliminary analyses determined that the introduction of a fourth parameter did not result in notable improvements for the Montana area.

The nonstationary GEV probability distribution function, as applied in Atlas 15, is defined as:

$$f(x,t) = \frac{1}{\sigma(x,t)}\left\{1 - \xi(x)\frac{x-\mu(x,t)}{\sigma(x,t)}\right\}^{\left(\frac{1}{\xi(x)}-1\right)} exp\left(-\left\{1 - \xi(x)\frac{x-\mu(x,t)}{\sigma(x,t)}\right\}^{\frac{1}{\xi(x)}}\right) \quad (1)$$

where μ, σ, and ξ are location, scale, and shape parameters, respectively, x is a spatial coordinate, and t represents time (year). For each region, the parameters are defined as follows

$$\text{Location:} \quad \mu(x,t) = a_1 \times MAM(x)\left[1 + a_2 \times GTI(t)\right] \tag{2}$$

$$\text{Scale:} \quad \sigma(x,t) = b_1 \times MAM(x)\left[1 + b_2 \times GTI(t)\right] \tag{3}$$

$$\text{Shape:} \quad \xi(x) = c_0 \tag{4}$$

The location and scale parameters (Eqns. 2 and 3, respectively) vary with a spatial covariate (MAM) and a temporal covariate (GTI; see Section 4.3.3 for more information on covariates). Because of its sensitivity to outliers, the shape coefficient is held constant (Eqn. 4) to avoid the generation of unreasonable values when modeling through time (OWP, 2022). In addition, a lower bound is imposed on the scale parameter (Eqn. 3) to ensure a non-negative result. The resulting parameters uniquely define a GEV distribution at each station within the domain for a given duration. This distribution provides precipitation frequency estimates for Volume 1 (PF_{VOL1}) under a range of AEPs for each respective station location.

4.3.2. Regionalization

Regional approaches, which use data from stations that are expected to have similar extreme precipitation characteristics, have been shown to yield more accurate estimates of extreme quantiles than approaches that use only data from a single station (e.g., Perica et al., 2018). The number of stations used to define a region should be large enough to smooth variability in at-station estimates, but also small enough that regional estimates still adequately represent local conditions. The regionalization process inherently contains a level of subjectivity. For example, selection of the maximum allowable distance from the point of interest, or choosing attribute variables (e.g., absolute elevation, relative elevation difference, etc.) and their roles in determining the weights imposed on individual stations.

In the Atlas 14 approach, stations were selected based on a maximum allowable distance from the station of interest. In addition, station selection was based on a combination of automatic and manual inspection of their locations with respect to mountain ridges, elevation differences, MAM differences at selected durations, and assessment of similarities/dissimilarities in the progression of relevant L-moment statistics across durations (e.g. 60-min, 2-hr, 3-hr, 6-hr, 12-hr, 24-hr, etc.).

While completely automated, the regionalization approach used for the Atlas 15 pilot largely mimics the Atlas 14 approach, with the exception that the Atlas 15 methodology applied a weighting scheme to regional stations based on similarity characteristics identified through the regionalization process. Because the number of daily and sub-daily stations varies significantly, regionalization was performed separately for durations of less than 24 hours and for durations equal to, or longer than, 24 hours. The regionalization approach used for the Atlas 15 pilot was as follows:

- For each station within the project area (target station), all stations within a 160-km radius from the target station (regional stations) were identified.

- Attributes for each regional station inside the 160-km radius were used to quantify its similarity to the target station. These were defined as the distance from the target station, the difference between MAP and MAM values for selected durations for the two locations, and the difference in their elevations. Additionally, elevation along a path was used to determine if a regional station is separated from the target station by complex terrain, such as a mountain ridgeline, resulting in two additional attributes: obstacle height and elevation range, as illustrated in Figure 4. Finally, two-sample Chi-squared and Kolmogorov-Smirnov tests were used to assess the extent of similarity in distributions between target and regional stations.

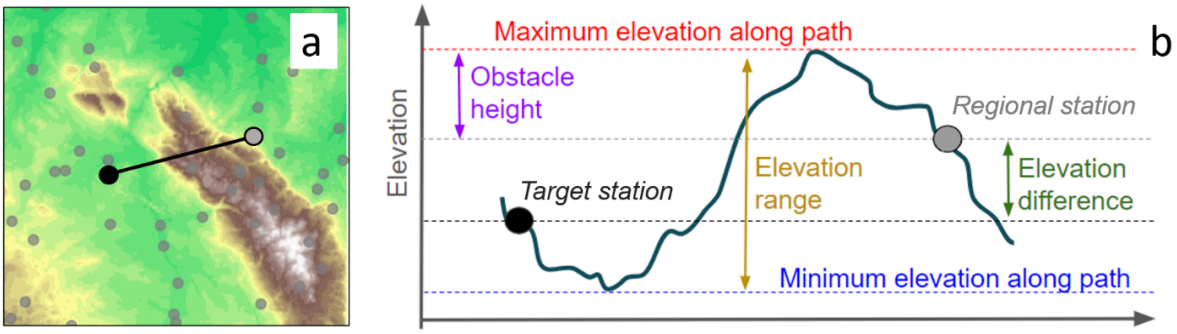

Figure 4. Definition of elevation attributes along a path between a target station (black dot) and regional station (gray dot) as depicted from above (a) and as a cross-section (b).

- For each attribute, minimum and maximum values were identified resulting in weights (W) of 1 or 0 that were applied to the corresponding AMS data when attributes fall outside this range. When attribute values fall within the specified range, W was derived using a triweight kernel function, resulting in a decrease from 1 to 0 as the attribute values approached the upper bound (see Table 2 and Figure 5). The bounds on the attribute ranges were estimated empirically based on their distributions within the pilot domain.
- The product of the attribute parameter weights was then used to compute a single weight, similar to the approach described by Daly et al. (2008), and applied to AMS data at each regional station, thus determining the extent of each regional station's contribution to the final estimate for the target station.

Table 2. Attribute parameters used in weighting of regional stations.

Attribute	$W = 1$	$1 > W > 0$	$W = 0$
Distance	x ≤ 70 km	70 < x < 160 km	x ≥ 160 km
MAP difference	x ≤ 70%	70 < x < 100%	x ≥ 100%
MAM difference	x ≤ 40%	40 < x < 75%	x ≥ 75%
Elevation difference	x ≤ 700 m	700 < x < 1200 m	x ≥ 1200 m
Obstacle height	x ≤ 600 m	600 < x < 1100 m	x ≥ 1100 m
Elevation range	x ≤ 1200 m	1200 < x < 1700 m	x ≥ 1700 m
P-value based on two-sample statistical tests	x ≥ 0.2	0.2 > x > 0.05	x ≤ 0.05

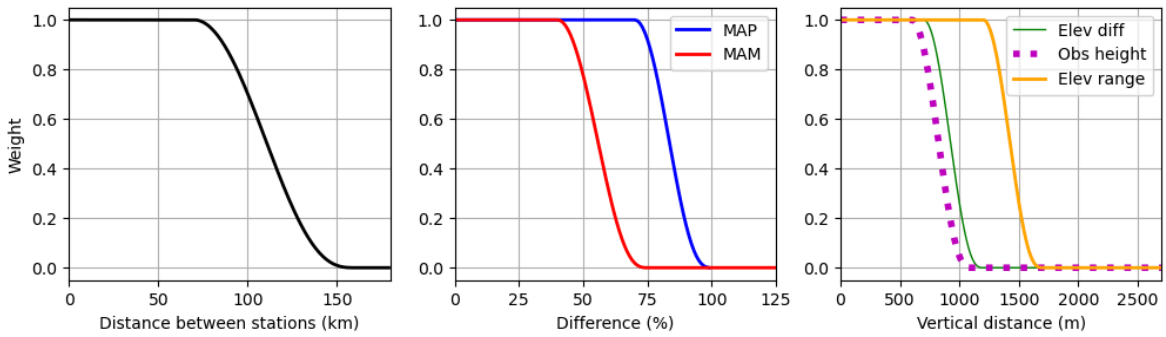

Figure 5. Depiction of weights based on selected attributes from Table 2.

An example of regional weighting around a target station is illustrated in Figure 6 for (a) hourly and (b) daily durations. Regional stations with weights close to 1 (black dots) are geographically closest to the target station and also have relatively similar precipitation attributes, with minimal terrain variability along the path between them and target station. Stations with weights of 0 (white) are either far from the target station, have different meteorological and geographical attributes, and/or are separated by complex terrain. Color gradations between white and black indicate stations with weights between 0 and 1. Note that if a regional station has a single attribute that is larger than the maximum allowable value ($W = 0$ column in Table 2), its final weight will also be zero, resulting in no contribution to the precipitation estimates at the target station.

4.3.3. Spatial and Temporal Covariates

As defined in Equations 2 and 3, spatial and temporal covariates were used to compute the location and scale parameters of the GEV distribution (Equation 1). Unique parameters, and thus unique GEV distributions, were defined for each station within the domain at each duration. Among several gridded spatial covariates that were tested (elevation, MAP, MAM, etc.), MAM had the best performance across all durations and was therefore retained as a spatial covariate for the Atlas 15 pilot domain.

For the temporal covariate, global CO_2 concentration and GTI were both investigated, and resulted in similar estimates for the present time (year = 2023). This similarity is not unexpected given the thermodynamic relationship between these variables and since greenhouse gas forcing (e.g., CO_2 concentration) is considered to be the dominant driver of global temperature changes since approximately 1960 (IPCC, 2023). As illustrated in Figure 7, the tested temporal covariates exhibit similar trends over this period which also coincides with the timing of the most abundant station data as shown in Figure 3(e). The result is nearly identical precipitation frequency estimates for the present year (2023) regardless of which covariate is used (with present-year $CO_2 \approx 419$ PPM and GTI ≈ 1.1 °C). For Volume 1, GTI was ultimately selected as the temporal covariate, defined as the 30-year moving average global temperature anomaly relative to the preindustrial period (1851 - 1900), thus ensuring consistency with Volume 2 (see Section 5).

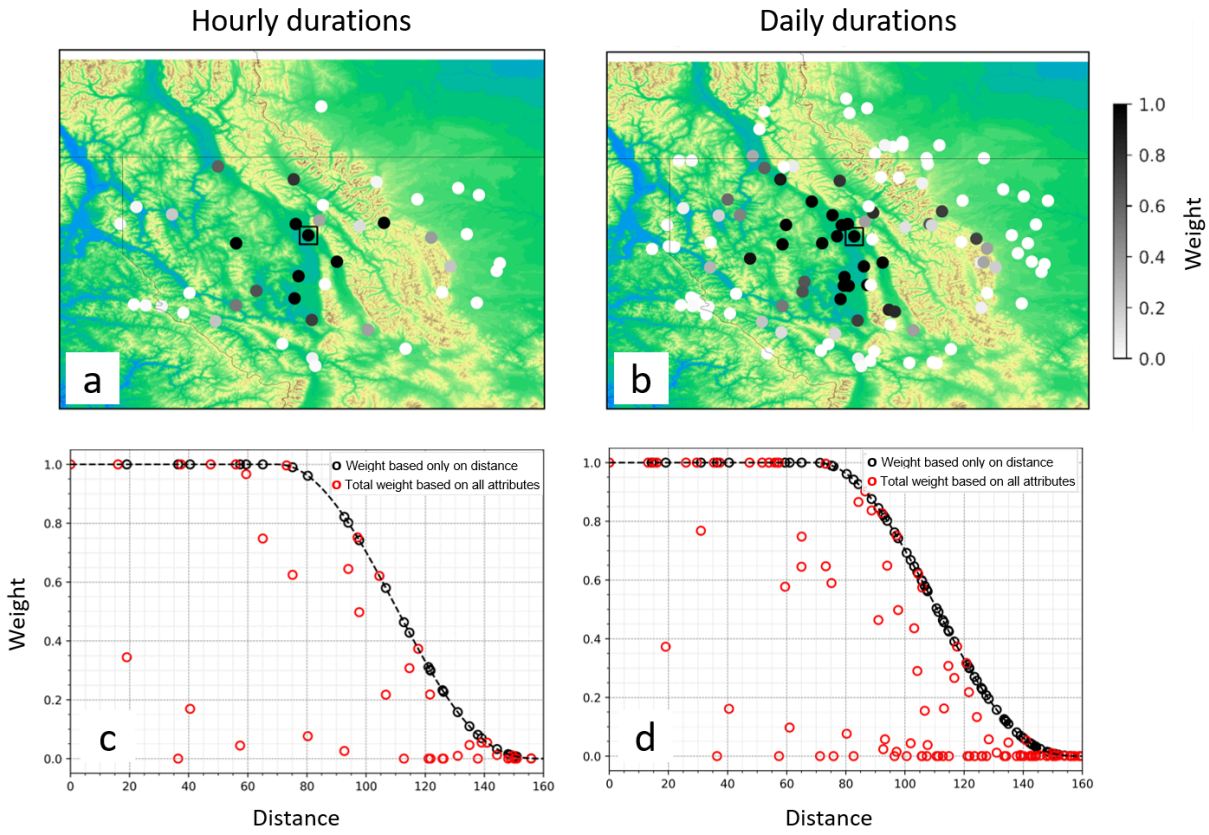

Figure 6. Example of regional weighting for hourly (a and c) and daily (b and d) durations, with the upper-bound determined by the distance weight (black points in c and d). Black dots in panels a and b show regional stations that contribute the most to estimations at the target station (encompassed by a black square), gray dots show stations with weights between 0 and 1, and white dots indicate stations with zero

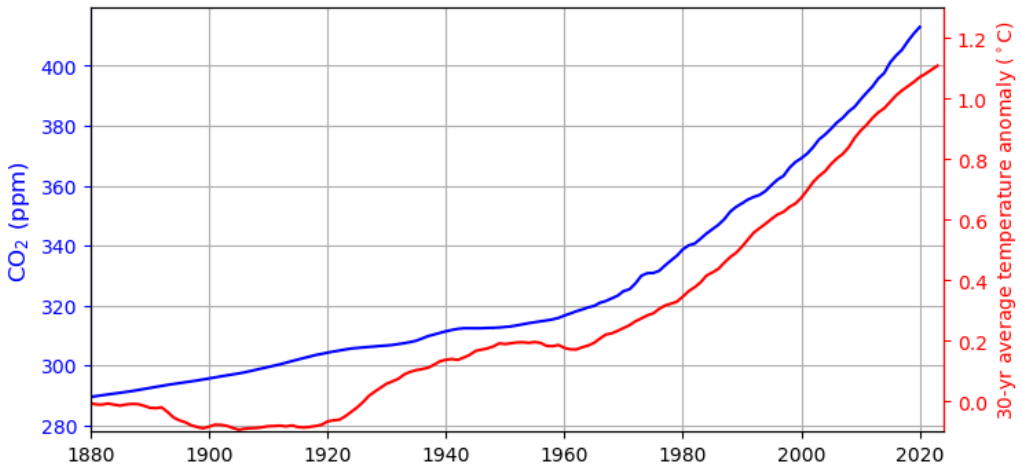

Figure 7. Temporal covariates examined for the Atlas 15 pilot framework, including global CO_2 obtained from the Coupled Model Intercomparison Project Phase 6 (CMIP6; Eyring et al., 2016) and GTI defined as the 30-year average global temperature anomaly (original data obtained from NCEI, 2023).

4.3.4. Interpolation to a Grid

The regionalization and statistical distribution fitting described above may either be performed at station locations or at the centers of each grid cell across the domain. Because the final Atlas 15 product is provided on a grid, the former approach requires an additional step of station-to-grid interpolation. Testing of both approaches resulted in similar final gridded values over Montana. However, grid-based estimation introduced some physically unrealistic artifacts between stations and did not permit use of the regional weight that depends on two-sample statistical test results (see Section 4.3.2). Moreover, performing the calculation of estimates at stations is far less computationally expensive than the calculation at gridded locations. For these reasons the station-based approach was adopted for Atlas 15.

Although the methodologies used to produce Atlas 14 Volume 12 and this pilot Atlas 15 product use different distribution parameterization methods to produce precipitation frequency estimates at rain gauge locations, the spatial interpolation approaches are conceptually similar. The technique takes advantage of the inherently strong linear relationship that exists between precipitation frequency estimates for consecutive AEPs and the MAM. For each duration, the calculation uses gridded MAM values as the predictor. At-station ratios between precipitation frequency estimates for a given AEP and corresponding MAM estimates are spatially interpolated to a grid using a monotonic cubic interpolation technique. Gridded MAM estimates are then multiplied by corresponding gridded ratios to create gridded precipitation frequency estimates. The same process is repeated for all hourly and daily durations identified in Table 1.

To ensure consistency in estimates across all durations and frequencies (e.g., 24-hour estimate has to be equal to, or greater than, the 12-hour estimate), duration-based internal consistency checks were conducted and in rare cases, adjusted as needed. Similar to the approach used for Atlas 14 (Perica et al., 2018), checks were performed on precipitation frequency estimates and their confidence bounds (see Section 4.3.5.), and was implemented at station locations and again at all grids following interpolation.

The resulting Atlas 15 Volume 1 pilot precipitation frequency estimates for 60-min and 24-hr durations and AEPs of 50%, 10%, and 1% are illustrated in Figure 8.

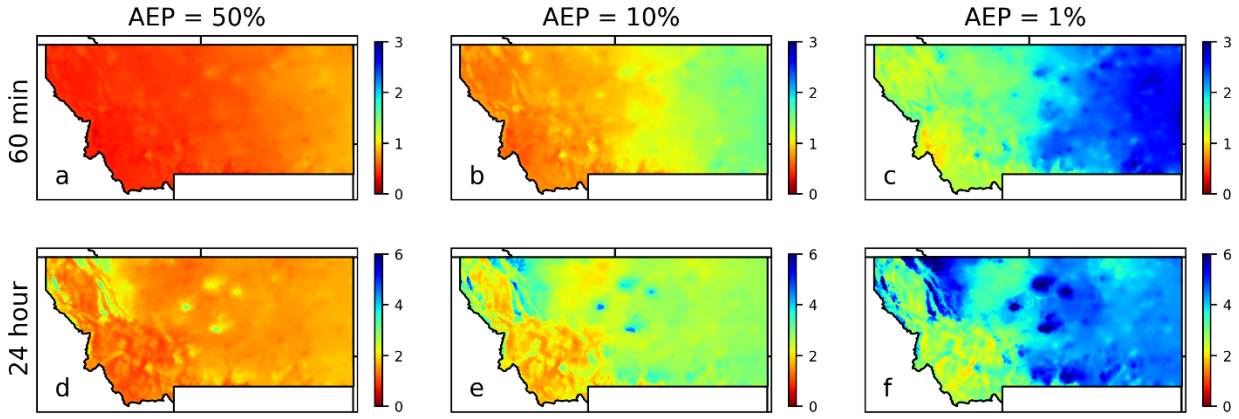

Figure 8. Atlas 15 Volume 1 pilot precipitation frequency estimates (PF_{VOL1}) for durations of 60 minutes (a-c) and 24 hours (d-f) with AEP of 50% (a and d), 10% (b and e), and 1% (c and f).

4.3.5. Confidence Intervals

A Monte Carlo simulation procedure that accounts for inter-station dependence was used to construct lower and upper bounds of 90% confidence intervals on AMS-based precipitation frequency curves. This was done by first adding random noise to MLE-derived GEV parameters at target stations, the magnitude of which is informed by the spread of individual-station parameter values within each region, thus accounting for uncertainty related to the estimation of regional parameters. This process was repeated 1,000 times resulting in an ensemble of unique distributions from which AMS values were randomly sampled, thus also accounting for uncertainties stemming from the stochastic nature of precipitation. Synthetic precipitation frequency estimates for each target station were generated from the distributions and sorted. Values corresponding to the 5% and 95% level were retained as confidence bounds.

This approach is similar to that used in NOAA Atlas 14 volumes (see for example Perica et al., 2018), however with two main differences: 1) Atlas 15 confidence interval estimates account for uncertainty in the GEV MLE parameters, while the Atlas 14 estimates account for uncertainty in L-moments; 2) inter-station dependence for each region was expressed as a function of distance in Atlas 15 in contrast to Atlas 14 where it was assumed to be uniform across the region.

4.3.6. Evaluation of Model Performance

When testing for goodness-of-fit for nonstationary extreme value models, common practice is to compare performance metrics between two or more models to determine which is best suited for the application. In the case of Atlas 15, stationary estimates can be obtained by setting the temporal covariate parameter coefficients in equations (2) and (3) to zero (i.e., $a_2 = 0$ and $b_2 = 0$), which can then be compared to nonstationary estimates. One performance metric, the Akaike Information Criterion (AIC), utilizes maximum likelihood to assess the balance between model fit and model complexity. Alternatively, the Corrected Akaike Information Criterion (AICc) takes sample size into account thus reducing an overfitting bias (e.g., Panagoulia et al., 2014; Kim et al., 2017). When assessing model fit, a lower relative score indicates a more optimal balance between parsimony and model performance. Given identical regional delineations and weights, the AICc provides a measure of added value with increased model complexity when accounting for nonstationarity.

Figure 9 illustrates (a) differences between 24-hour precipitation frequency estimates under preindustrial and present-day GTI values, and (b) differences between AICc scores for the nonstationary and stationary models for 1% AEP at present time (year = 2023), with dashed lines indicating areas with significantly improved performance ($p < 0.05$) by the nonstationary model according to a Likelihood Ratio Test (LRT). Because AICc imposes a penalty on models with more parameters, even if equivalent model performance is achieved, the stationary model would be granted a lower (better) score than the nonstationary model. This is due to the nonstationary model's inclusion of additional parameters, associated with the temporal covariate, when estimating the location and scale parameters, thus making it a more complex model.

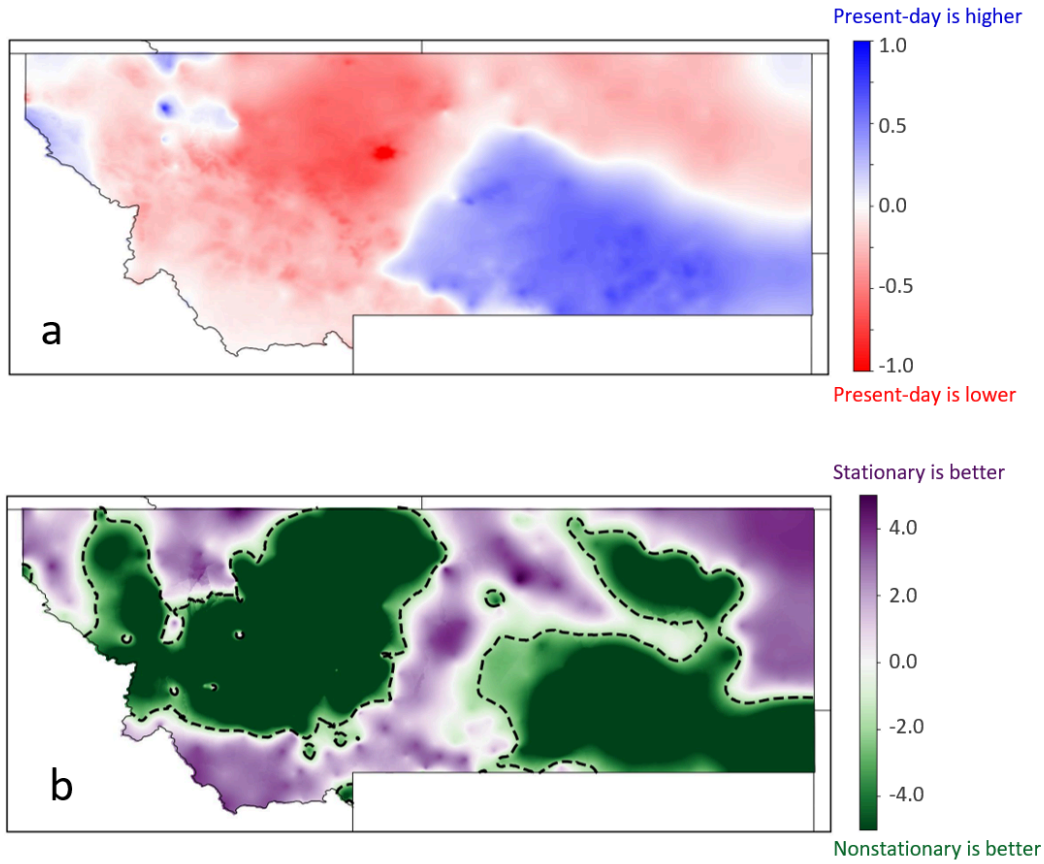

Figure 9. (a) Difference in estimated 24-hr precipitation (inches) for AEP = 1% between GTIs of 1.1°C (approximate GTI in 2023) and 0°C (preindustrial), where red and blue indicates drier and wetter present-day conditions, respectively; (b) differences in AICc scores for stationary and nonstationary models, where purple and green indicate that either the stationary model or nonstationary model is "better," respectively, with dashed lines encompassing areas where a significant ($p < 0.05$) improvement in nonstationary model performance was observed based on a likelihood ratio test.

The areas of dark green in Figure 9(b) generally coincide with areas of largest changes in 24-hr precipitation frequency estimates for AEP of 1% indicated by deep blues and reds in (a), suggesting that the nonstationary model provides better fit than the stationary model in areas where precipitation changes are greatest, as expected. The areas of dark purple in (b) generally coincide with little-to-no change in precipitation in (a), indicating that the nonstationary model is unnecessarily complex in these areas. This analysis illustrates the flexibility of the nonstationary model. While the additional terms in the nonstationary model may not be necessary in areas absent of trends, the added value of the nonstationary term transcends the penalty imposed from increased complexity in areas where trends do exist. As Atlas 15 is expanded beyond the Montana domain, it is expected that greater, and largely positive, extreme precipitation trends will be encountered, particularly toward the Midwest and eastern areas of the U.S. (e.g., Marvel et al., 2023). This underscores the need for a model that accounts for nonstationarity when estimating current extreme precipitation conditions (e.g., Cheng and AghaKouchak, 2014; Vu and Mishra, 2019; Feitoza Silva et al., 2021).

4.3.7. Comparison with Atlas 14 Volume 12 estimates

Figure 10 illustrates differences in estimates for 60-minute and 24-hr durations for an AEP of 1% between the stationary Atlas 14 and the nonstationary Atlas 15 estimates. The differences are generally within about 20% and do not appear to be related to geographical features. The largest differences are attributed to the use of a nonstationary model for Atlas 15. Comparison of the 24-hr differences in Figure 10 (c and d) and Figure 9 (a) reveals consistent spatial patterns. In areas where the Atlas 15 nonstationary present-day estimates are higher (lower) than preindustrial values, the Atlas 15 estimates also are generally higher (lower) than the Atlas 14 estimates. It can thus be concluded that differences between Atlas 15 and Atlas 14 are largely due to the use of a nonstationarity framework.

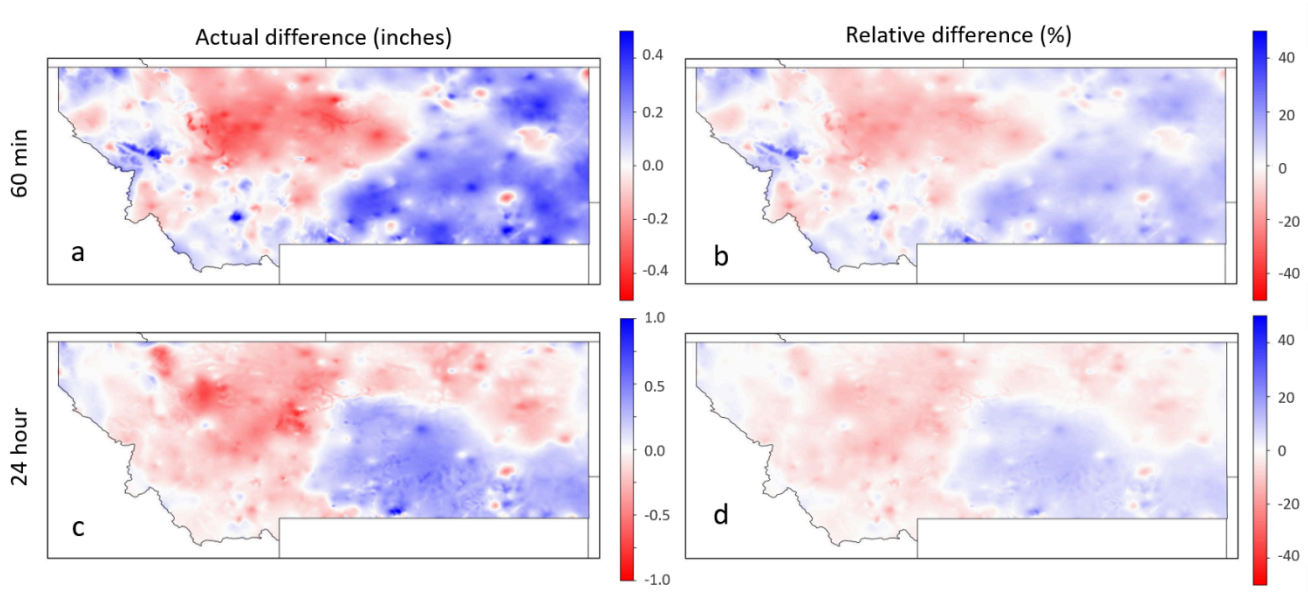

Figure 10. Differences between Atlas 15 Volume 1 and Atlas 14 60-min and 24-hr precipitation frequency estimates (PF_{VOL1}) for AEP of 1% expressed as inches (a,c) and as percent (b,d). Blue indicates areas of higher Atlas 15 values and red indicates areas of higher Atlas 14 values.

5. NOAA Atlas 15 Pilot Volume 2

5.1. Background and Overview

5.1.1. Impacts of Global Temperature on Extreme Precipitation

Research over the past several decades has informed our understanding of the effects of global temperature changes on heavy precipitation. Regular assessments of research by the international community through the Intergovernmental Panel on Climate Change (IPCC) and the national community through the U.S. National Climate Assessment (NCA) effort of the U.S. Global Change Research Program (USGCRP) provide syntheses of this understanding. These syntheses are the outcome of meticulous and exhaustive work by large teams of subject matter experts, and undergo multiple rounds of external review. The 2nd, 3rd, 4th, 5th, and 6th Assessment Reports of the IPCC all addressed the topic of heavy precipitation, as do all five NCA assessments [see IPCC (2023) and USGCRP (2023) for the latest reports, respectively]. These syntheses have consistently stated the likelihood of general increases in heavy precipitation in response to higher temperatures . The latest (Sixth) IPCC assessment states that “heavy precipitation will generally become more frequent and more intense.” Specifically, it is extremely likely that the intensity and frequency of heavy precipitation events will increase in North America with global temperatures of 2°C above preindustrial values (Seneviratne et al., 2021), which is largely due to the expected increase in atmospheric water vapor according to the Clausius-Clapeyron relationship. The latest (Fifth) U.S. NCA concludes that “the frequency and severity of heavy precipitation increases with the [global temperature index]” (USGCRP, 2023). Furthermore, a recent report by the National Academies of Science, Engineering and Medicine (NASEM) on probable maximum precipitation provided a recent review of research and the implications for very extreme precipitation. It stated, “the assumption that climate change does not affect extreme rainfall, implicit in traditional stationary analysis, is contrary to multiple lines of evidence. Neglecting climate change generally underestimates both present-day and future risk of extreme rainfall”. This report further states that “scientific confidence in climate-driven changes in extreme weather depends on three separate lines of evidence: a clear trend in observations, a clear trend in climate model simulations, and physical understanding of the connection between climate change and extreme trends, with confidence highest if all three lines present” (NASEM, 2024).

5.1.2. Climate Models

The quantitative effect of global temperature changes on precipitation frequency values is a function of several atmospheric physical processes and varies by location, duration, and AEP. Summaries of these effects and dependencies can be found in the IPCC Sixth Assessment Report [Chapter 11, Seneviratne et al. (2021)], O’Gorman (2015), and Neelin et al. (2022). General circulation model (GCM) simulations and their downscaled regional derivatives are used to quantify these effects. Because raw GCM data are generally only available at coarse spatial resolutions (50 - 250 km) and are often characterized by biases, many applications require downscaling to allow for the extraction of localized data, such as extreme precipitation, for which major biases have been removed. The process of downscaling using statistical methods also introduces high resolution spatial detail into the precipitation climatology. Statistical downscaling models are developed by comparing raw GCM data with observational datasets. However, for projected values, downscaling models have only raw GCM projections to constrain their values (there is no future equivalent to the observed values for the historical climatology). Thus, there is no information at scales smaller than the resolutions of the GCMs. This is not the case for dynamically-downscaled datasets. Since dynamical downscaling models are regional equivalents to the GCMs in terms of their representation of atmospheric physical

processes, they can simulate smaller-scale physical features. A prime example is topography where some key physical processes, such as downwind moisture shadowing and topographic uplift enhancement will be more realistically portrayed in a regional climate model. However, these models are much more computationally expensive than statistically downscaling models. Thus, the number and variety of datasets is much more limited.

Based on these considerations, the robustness of information on spatial variability of future projections at scales smaller than the typical GCM grid cell size was judged by the authors of Volume 2 to be insufficient for incorporation into the Atlas 15 pilot. The adjustment factors applied here were thus smoothed over scales of a few hundred kilometers (a few grid cells) to produce robust estimates at regional scales. Because of this smoothing, application of the adjustment factors (as described in the next section) do not change the relative small-scale spatial structure of the estimates obtained for Volume 1.

5.1.3. Adjustment Factor Frameworks

Future values for Volume 2 (PF_{VOL2}) were developed by applying adjustment factors to the Volume 1 estimates (PF_{VOL1}). The adjustment factors were calculated for two frameworks: global temperature index (GTI) and scenarios (i.e. climate model emissions scenarios). In the GTI framework, which is comparable to the framework used extensively in the IPCC 6th Assessment Report (IPCC, 2023), adjustment factors are calculated for the years in which each model's global-average temperature reaches specified temperature anomalies (degrees above a baseline). A key assumption for use of the GTI framework is that precipitation frequency at a specified GTI is independent of the year during which it occurs due to the rapid response of atmospheric water vapor uptake to change in temperature. It is thus expected that similar values per GTI would be obtained between different models, and even when driving models are forced with different emission scenarios (i.e., SSP2-4.5, and SSP5-8.5). There are some limitations of this assumption that mostly relates to whether the temperature of land and surrounding oceans, and its relationship to the global average temperature change, differ between the faster-warming and slower-warming simulations. At this time, there is no evidence of this, so for simplicity, the independence assumption is made for the present application. This approach tends to show smaller model spread than for fixed times (i.e., for the year 2060). Figure 11 shows time series of global average temperatures under the SSP5-8.5 scenario for 16 models used in the creation of the statistically-downscaled datasets discussed in the next section. As an example, the year at which these models reach 3°C of warming varies from 2040 to 2078.

In the scenario framework, adjustment factors represent the conditions for a particular decade under a specified future scenario. Scenarios reflect what is referred to as Shared Socioeconomic Pathways (SSP) and represent a combination of changes in future conditions including population, economic growth, and the resulting greenhouse gas emissions and land-use changes (O'Neill et al., 2017). In the example presented in Figure 11, for the SSP5-8.5 scenario, the conditions for the year 2060 include contributions from models with warming ranging from a little over 2°C to over 4°C. The two scenarios chosen here for future precipitation frequency values, SSP2-4.5 and SSP5-8.5, are considered intermediate and very high scenarios, respectively (Jay et al., 2023). These represent a multi-model mean global temperature index of about 3°C and about 5°C, relative to preindustrial conditions, by the end of the 21st Century (Lee et al. 2021). Note that there are also two lower-emissions scenarios, SSP1-1.9 and SSP1-2.6. In these scenarios, the global temperature is nearly constant through the 21st Century (Lee et al. 2021). Thus, for Atlas 15 applications needing low scenarios, our 1.5°C and 2.0°C GTI results provide a suitable approximation.

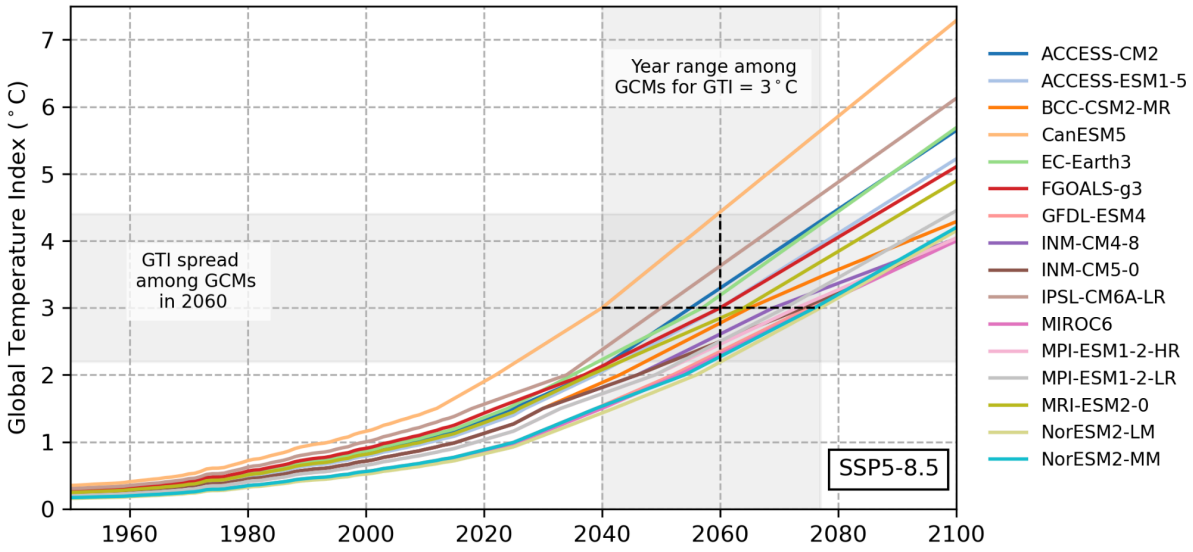

Figure 11. Time series of global average temperature anomaly, with respect to 1851-1900, for the 16 models used in the downscaling datasets.

5.2. Relevant Datasets

Table 3 lists characteristics of the datasets planned for use in the development of the Atlas 15 Volume 2 adjustment factors. Due to limits on the availability of data at the time of analysis, the Montana pilot adjustment factors were based on an analysis of only three of these datasets, LOCA2, STAR, and NA-CORDEX, which are discussed below. Final Atlas 15 adjustment factors will be based on an analysis of all of the datasets identified in Table 3.

Table 3. Characteristics of datasets planned for use in development of adjustment factors for the Atlas 15 Volume 2 CONUS domain.

Downscaling Approach	**Statistical, based on CMIP6**			**Dynamical, based on CMIP6**	**Dynamical, based on CMIP5**	**Dynamical, based on CMIP5**	**Large Ensembles**	
Target	**Daily durations**			**Sub-daily durations**			**Low AEPs**	
Dataset	LOCA2[1]	STAR-ESDM[2]	UWPD[3]	CONUS404[4]	NIU[5]	NA-CORDEX[6]	GFDL-SPEAR[7]	CESM-LENS[8]
Spatial Resolution	1/16°	1/24°	1/10°	4 km	3.75 km	25 km	50 km	1°
Temporal Resolution	Daily	Daily	Daily	15-min	15-min	Hourly	Daily	6-hourly* and daily
Temporal Domain	1950-2100	1950-2100	1950-2100	1979-2021 2022-2064	1990-2005 2041-2055 2085-2100	1950-2100	1921-2100	1920-2100
Scenarios	SSP2-4.5 SSP5-8.5	SSP2-4.5 SSP5-8.5	SSP2-4.5 SSP5-8.5	SSP3-7.0	RCP4.5 RCP8.5	RCP4.5 RCP8.5	SSP5-8.5	RCP8.5

[1] LOCA2 - Localized Constructed Analog v2
[2] STAR-ESDM - Seasonal Trends and Analysis of Residuals Empirical-Statistical Downscaling Model
[3] UWPD - University of Wisconsin Probabilistic Downscaling
[4] CONUS404 - USGS CONterminous U.S. 404 high-resolution hydro-climate dataset
[5] NIU - Northern Illinois University Convection-Permitting
[6] NA-CORDEX - North American Coordinated Regional Downscaling Experiment
[7] GFDL-SPEAR - Geophysical Fluid Dynamics Laboratory-Seamless System for Prediction and EArth System Research
[8] CESM-LENS - Community Earth System Model-Large Ensemble Community Project
* 6-hourly data are available for three time periods: 1990-2005, 2026-2035, 2071-2080.

Two statistically downscaled products were used to generate future adjustment factors at daily durations. Both products, LOCA2 (Pierce et al., 2014 and 2023; https://downscaling.lbl.gov/data/) and STAR-ESDM (Hayhoe et al., 2023), are generated through statistical downscaling of Coupled Model Intercomparison Project Phase 6 (CMIP6) data (Eyring et al. 2016; https://pcmdi.llnl.gov/CMIP6/). LOCA2 and STAR-ESDM data are generated with deterministic statistical models that employ empirical relationships between synoptic- and local-scale historical spatial patterns and temporal signals. Both products are available at a daily temporal resolution for 1950-2100 and at spatial resolutions of 1/16th degree (LOCA2) and 1/24th degree (STAR-ESDM). For the present work, data were extracted from 16 unique GCMs that were downscaled by both modeling groups, resulting in 32 ensemble members. This analysis used only the shared socioeconomic pathway 5-8.5 (SSP5-8.5), which excludes mitigation, because it has the highest range of greenhouse gas emissions among the scenarios used in CMIP6. This scenario thus maximizes the sample size of the number of models that reach specified GTIs.

Both LOCA2 and STAR-ESDM were also used in the Fifth National Climate Assessment (NCA5) which was released in 2023 (USGCRP 2023). Figure 12 describes the framework for scaling low-resolution global data from CMIP6 (left side of the diagram) down to bias-adjusted high-resolution products (right side of the diagram) used in NCA5. The two downscaling algorithms (center of the diagram), LOCA2 and STAR-ESDM, were developed for each of the 16 selected GCMs (shown in dark blue) by training with two observational datasets (Livneh for LOCA2 and nClimGrid for STAR-ESDM; shown in green). The resulting algorithms produce high-resolution bias-adjusted datasets of daily temperature and precipitation for the training dataset's observational period. These model-specific algorithms are applied to global projections to produce high-resolution projections of temperature and precipitation in the United States for each model (shown in light blue). Both LOCA2 and STAR-ESDM provide gridded data for the 48 contiguous states, and STAR-ESDM additionally includes downscaled data for individual stations in Alaska, Hawai'i, and Puerto Rico.

In general, adjustment factors are a function of storm duration. There are several climate model datasets available to support estimates for daily and longer durations, but because there are fewer datasets available at sub-daily resolutions, this sample size is much smaller. The methodological approach for Atlas 15 is to use sub-daily resolution climate model datasets to explore the relationship of sub-daily adjustment factors to daily adjustment factors. Because sub-daily CMIP6 data are not currently available, the NA-CORDEX archive, which includes various dynamically downscaled CMIP5 products (Mearns et al., 2017; https://na-cordex.org/) was used to examine the relationship between daily and sub-daily adjustment factors. A total of 7 downscaled simulations were used, representing selected combinations of 4 driving CMIP5 GCMs and 3 regional climate models.

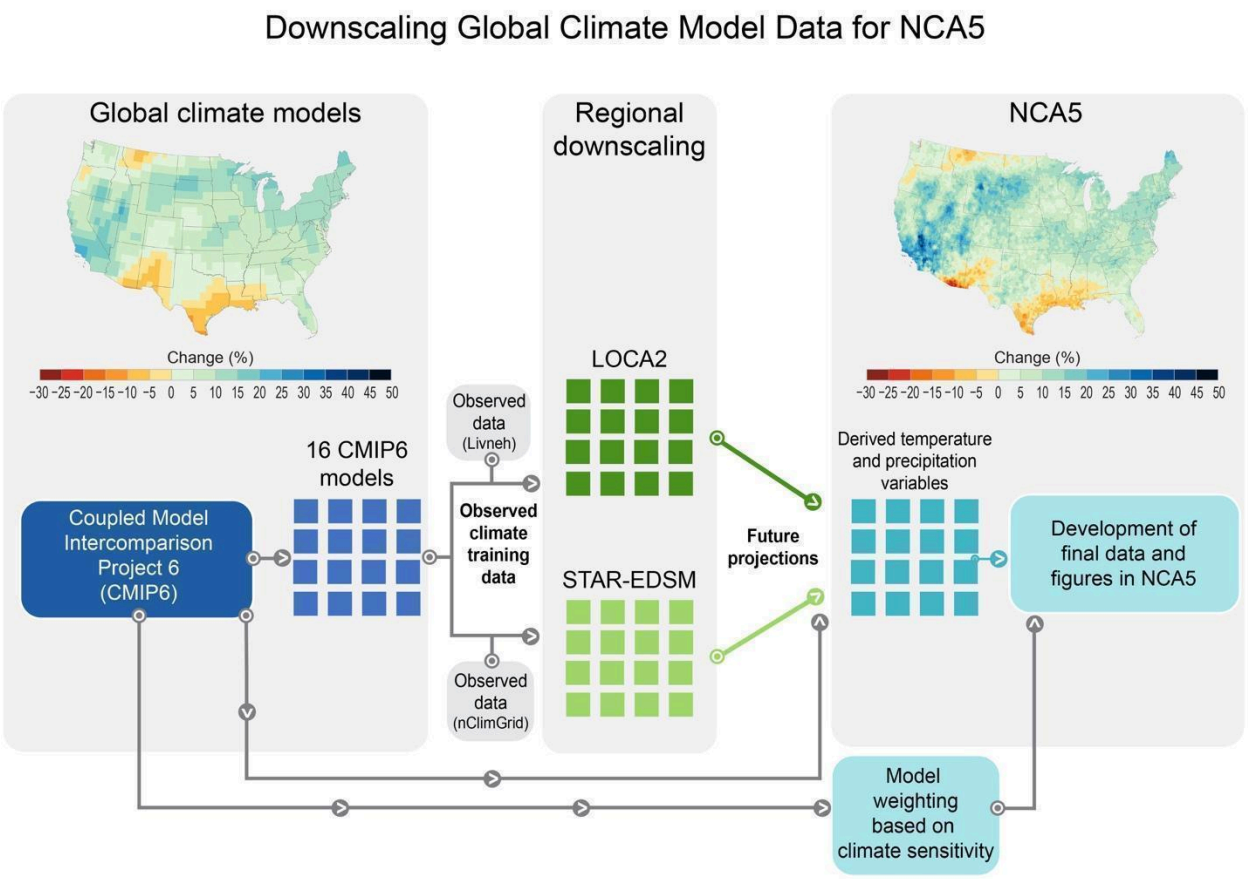

Figure 12. Flowchart illustrating the steps taken to downscale low-resolution global data from CMIP6 (left side of the diagram) to bias-adjusted high-resolution NCA5 products (right side of the diagram). Figure credit: USGCRP/ICF, USGCRP, and North Carolina State University. Taken from Basile et al. (2023).

5.3. Methods

5.3.1. Computation of Adjustment Factors

Unlike Volume 1 which utilized historical station gauge data, the GEV distribution parameters for the Volume 2 pilot were estimated using gridded AMS values extracted from LOCA2 and STAR-ESDM. The location, scale, and shape parameters, which are computed in a similar manner as Volume 1 (see Section 4.3.), are thus identified for every grid cell within the domain and for each of the 32 ensembles for daily and longer durations during the 1950 – 2100 period (see Section 5.3.2 for details regarding sub-daily storm durations). The resulting GEV distributions were used to generate precipitation frequency estimates at grid cell resolutions native to each statistical model. Thus, while the Volume 1 estimates originate at station locations, with one value per duration and AEP, the Volume 2 estimates originate on a grid, with 32 values (one from each model ensemble) per duration and AEP.

Once absolute precipitation frequency estimates were obtained for each GTI (1.5 - 5°C), their changes, relative to a baseline year of 2023, were computed. Figure 13 conceptually illustrates this relationship using a GTI of 3°C. Note that this example includes the model-average GTI for simplicity, but that the actual adjustment factors were instead computed for each individual model. Here, precipitation frequency estimates are generated for the present (2023) and then again for a future time when the GCMs reach 3°C. Adjustment factors represent the difference

in precipitation frequency estimates between these times, and thus provide estimates for PF_{VOL2} when applied to PF_{VOL1} as described in Section 5.3.3.

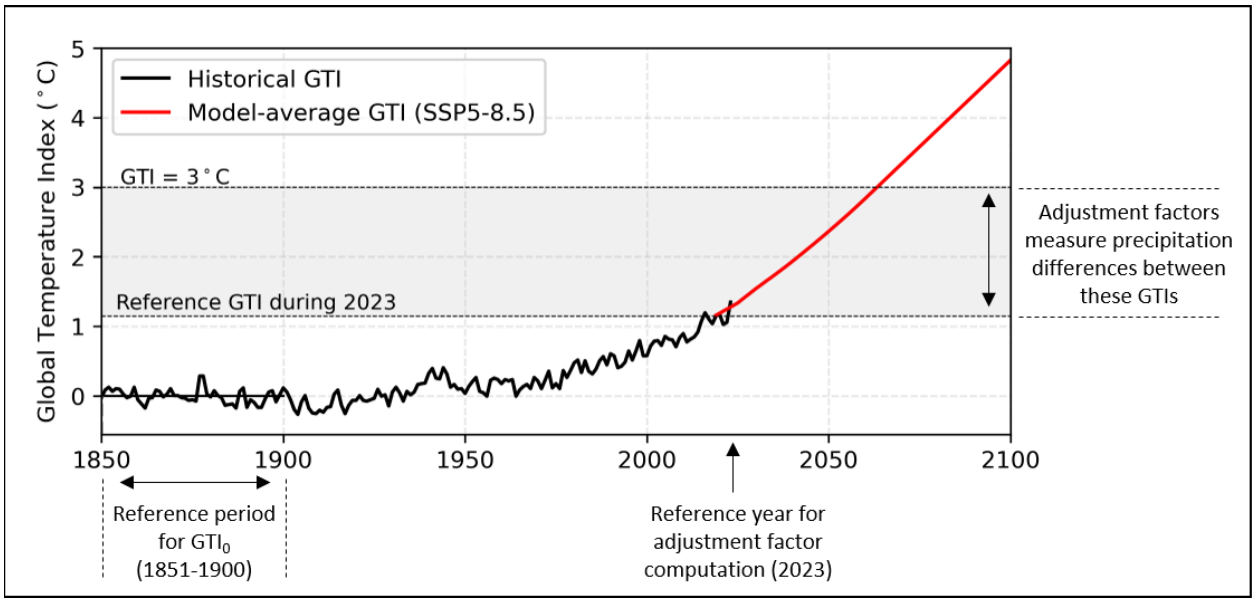

Figure 13. Conceptual illustration of how adjustment factors are computed for GTI = 3°C. The black line illustrates GTIs during the historical period and the red line illustrates model-average GTIs for the future. Multi-model adjustment factors are computed as the relative differences between precipitation estimates obtained during 2023 and those obtained when the models reach 3°C.

After adjustment factors were computed, a Gaussian filter was used to smooth their spatial variability and the data were regridded to a common 0.1° resolution. For each 0.1°grid cell in the pilot domain, there were 32 adjustment factor values per duration, AEP, and GTI, each resulting from a separate model ensemble member. These factors were then averaged across the models and used to estimate 90% confidence intervals which represent model spread.

5.3.2. Revision of Sub-Daily Adjustment Factors

Due to small sample sizes, rather than use sub-daily adjustment factor estimates that may be extracted from dynamically-downscaled climate model data directly, their relative relationships to the daily adjustment factors, which are based on much larger sample sizes, were applied. This makes use of the physics-based processes in the dynamically-downscaled climate model simulations, such as those available in the NA-CORDEX archive, but avoids the possibility that the absolute adjustment factors from the small number of sub-daily simulations may not be representative of the much larger daily data ensemble. This preserves internal consistency across all durations.

For the pilot framework, relative relationships between daily and sub-daily adjustment factors were generated based on an investigation of differences between projected changes in daily and sub-daily extreme precipitation according to the NA-CORDEX archive. Because these data are produced with high-resolution dynamical models, they are more likely to capture changes in small-scale convective precipitation which may make a greater contribution to total precipitation at sub-daily durations than at daily-and-longer term scales.

5.3.3. Application of Adjustment Factors

The resulting area-averaged adjustment factors for durations of 60 minutes, 24 hours, and 10 days, and AEPs of 50% and 1%, under a range of global temperature indices , are illustrated in Figure 14. The spatial patterns of 24-hr duration adjustment factor values under a range of AEPs are illustrated in Figure 15 for GTIs of 1.5°C and 5°C. The smoothed values do not resolve small-scale features, such as terrain, thus ensuring that such information from Volume 1 data will be preserved in the final Volume 2 estimates.

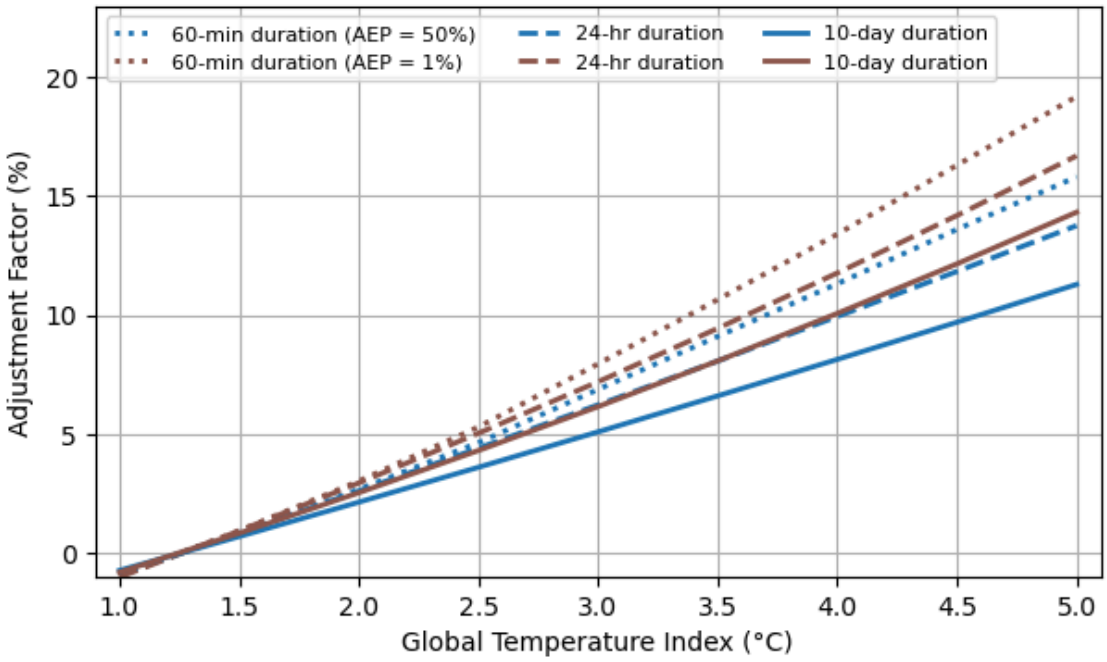

Figure 14. Atlas 15 Volume 2 area-averaged adjustment factors (%) for AEPs = 50% and 1% per GTI for 60-min, 24-hr and 10-day durations.

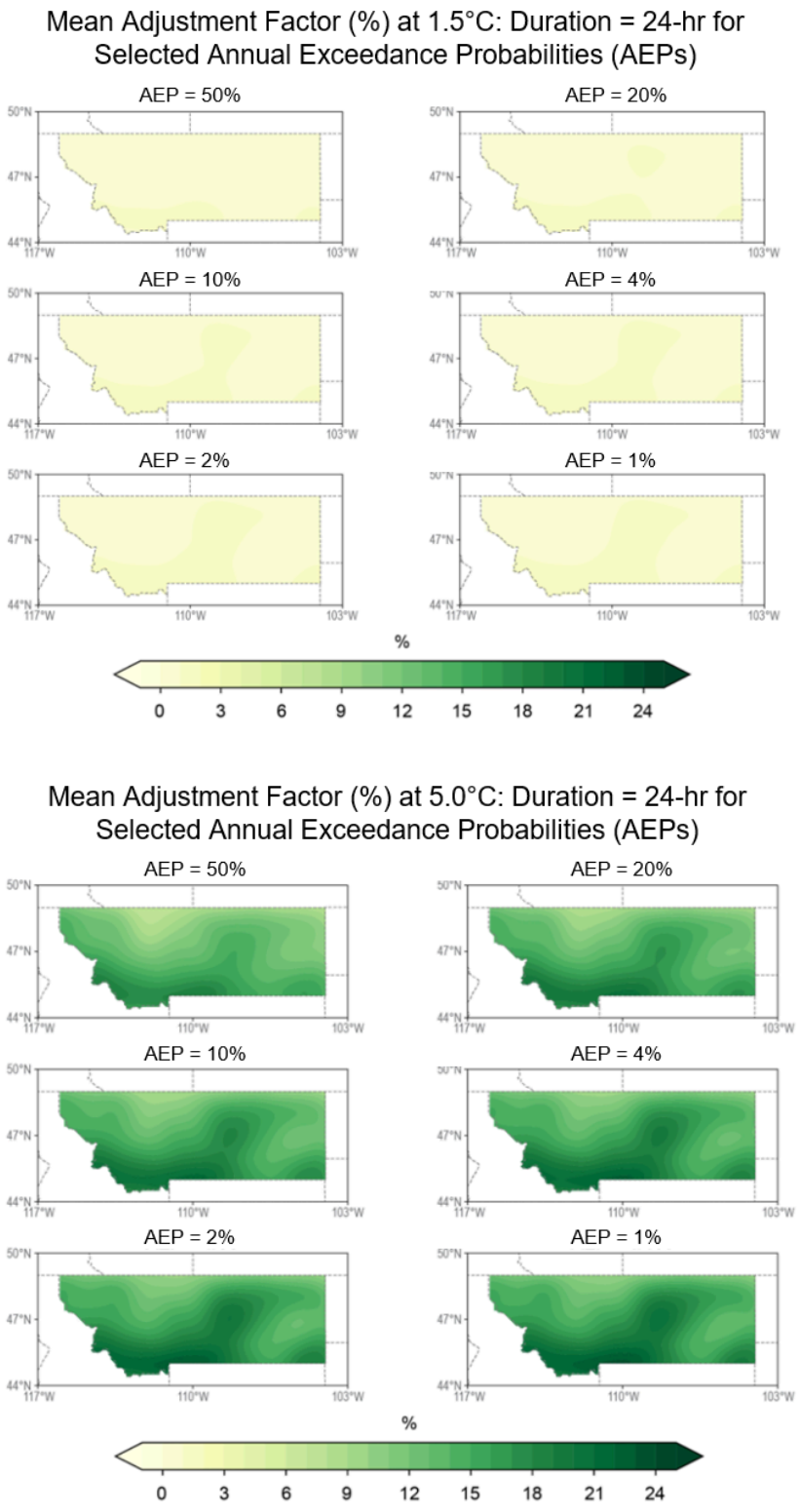

Figure 15. Atlas 15 Volume 2 adjustment factors for 24-hr duration and a range of AEPs under GTIs of 1.5°C (top) and 5°C (bottom). These adjustments are with respect to the current global temperature

relative to 1851-1900, which is 1.1°C. Thus, these adjustments are for further warming of 0.4°C and 3.9°C.

Once daily and sub-daily adjustment factors were calculated in the GTI framework, they were calculated in the scenario framework by mapping them to individual decades during 2030 – 2100 under SSP2-4.5 and SSP5-8.5. For this mapping, the multi-model mean GTIs per decade under each scenario were calculated. The gridded adjustment factors and confidence intervals were identified at the two GTIs nearest to those for each decade and scenario, and scenario-based values were then obtained through interpolation.

Future precipitation frequency estimates (PF_{VOL2}) were developed by applying the resulting adjustment factors (*AFs*), as defined under both the GTI and scenario frameworks, to the Volume 1 estimates (PF_{VOL1}). Specifically, for each duration,

$$PF_{VOL2}(x,t) = (1 + 0.01 \times AF(x,t)) \times PF_{VOL1}(x) \quad (5)$$

where AF values are functions of space x and time t dependent on GTI, emissions scenarios, and AEP. The multiplicative term is based on an adjustment factor that expresses (in units of percent) the relative change in the future from the PF_{VOL1} baseline which represents the year 2023. Thus, the final PF_{VOL2} values represent future precipitation estimates for the same durations and AEPs as PF_{VOL1}, but are also functions of global temperature (GTI framework) and time (scenario framework).

The 90% confidence interval bounds for Volume 2 adjustment factors, which were estimated from the model spread, were combined with the Volume 1 values to obtain the Volume 2 confidence bounds. The final Volume 2 values are thus expressed as precipitation depths, as with those for Volume 1, for all durations and AEPs.

6. NOAA Atlas 15 Precipitation-Frequency Estimates Over Montana

The final Volume 1 and Volume 2 estimates are packaged as Zarr files defined in Table 4. The time dimension for the Volume 1 file (*A15_Vol1.zarr*) has a length of one, which represents present-day values, while the Volume 2 scenario framework files (*A15_Vol2_SSP245.zarr* and *A15_Vol2_SSP585.zarr*) have lengths of eight (one per decade from 2030 until 2100) and the Volume 2 GTI file (*A15_Vol2_GWL.zarr*) has a length of nine (one per temperature level). The remaining attributes have the same characteristics across both volumes and frameworks.

Table 4. Description of data for Volume 1 and Volume 2 Zarr files.

	Volume 1	Volume 2	
Framework	***n/a***	**GTI**	**Scenarios (SSP2-4.5 and SSP5-8.5)**
File name	*A15_Vol1.zarr*	*A15_Vol2_GWL.zarr*	*A15_Vol2_SSP245.zarr* *A15_Vol2_SSP585.zarr*
Attribute - name (length)	Time - time (1)	GTI - gwl (9)	Time - time (8)
	Estimates and confidence limits - climit (3) Duration - dur (11) Annual exceedance probability - aep (6) Latitude - lat (591) Longitude - lon (1473)		

Spatial plots of selected precipitation frequency estimates for AEP of 1% under Volume 1 (current estimates as of 2023) and Volume 2 (GTI = 3 and 5°C) are illustrated in Figure 16. The location of Helena, Montana is indicated by the black x, for which depth-duration-frequency (DDF) curves are illustrated for Volume 1 in Figure 17, with projected changes under Volume 2 for select GTIs and AEPs in Figure 18. Precipitation estimates with 5% and 95% confidence bounds for 24-hr and AEP of 1% are illustrated in Figure 19.

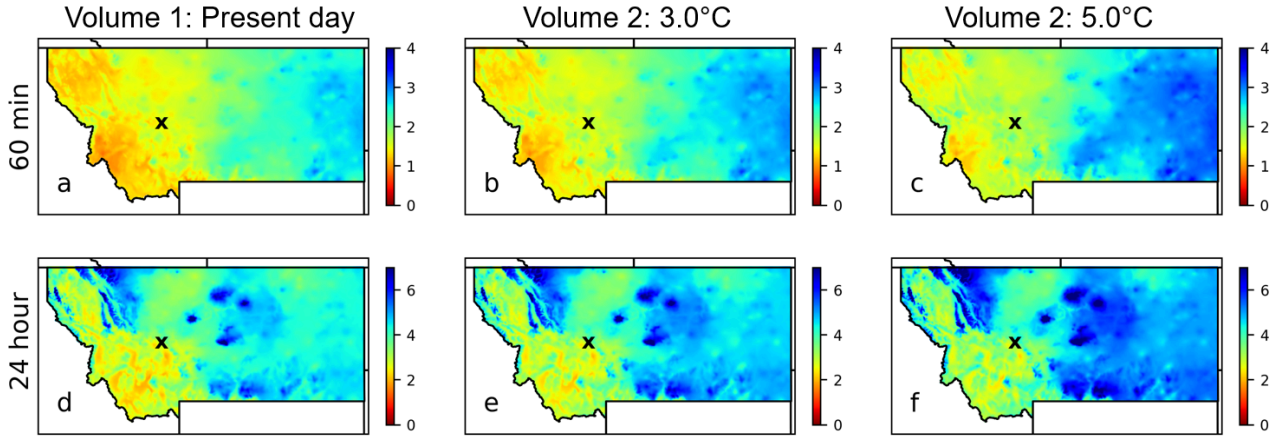

Figure 16. Atlas 15 precipitation estimates (inches) for AEP of 1% and durations of 60 minutes (a-c) and 24 hours (d-f) for Volume 1 (a and d), and Volume 2 GTI = 3°C (b and e) and 5°C (c and f). Black x indicates the location of the Helena, MT station which is used as an example in Figures 17 and 18.

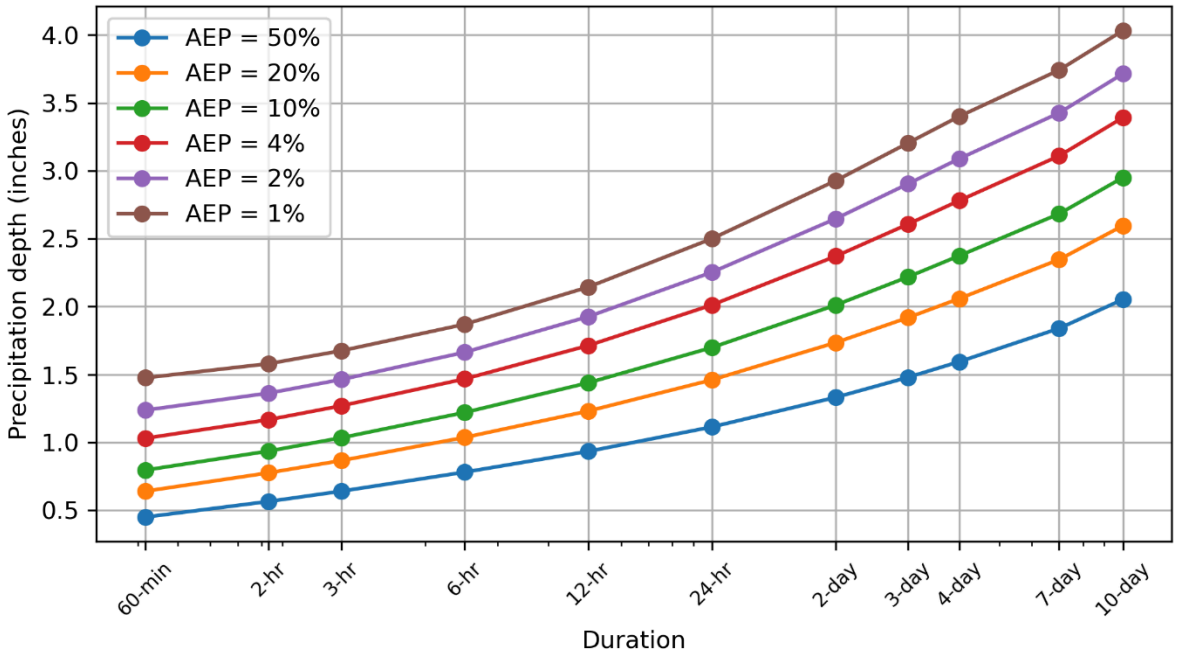

Figure 17. Atlas 15 Volume 1 depth-duration-frequency curves for selected durations and AEPs at Helena, Montana (112.0 W,46.6 N).

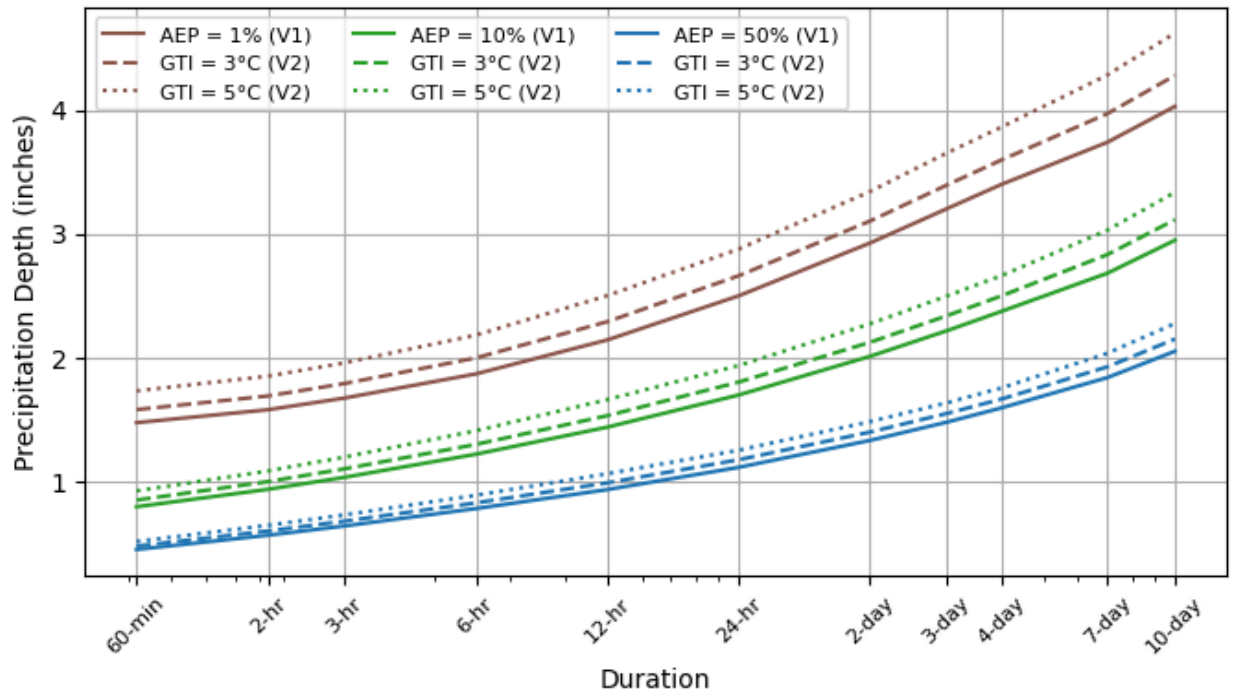

Figure 18. Atlas 15 depth-duration-frequency curves for selected durations and AEPs at Helena, MT (112.0 W,46.6 N) for Volume 1 (present) and Volume 2 (GTI = 3°C and 5°C).

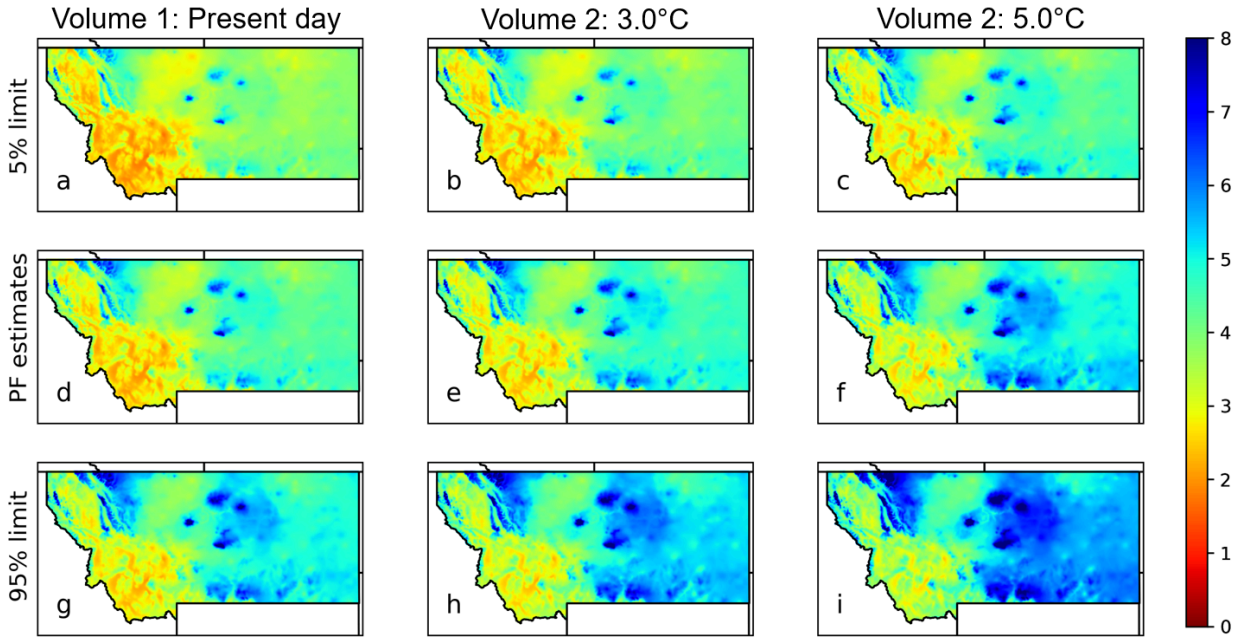

Figure 19. Atlas 15 precipitation frequency estimates (inches) for AEP of 1% and 24-hr duration (d-f), with 5% (a-c) and 95% (g-i) confidence limits for Volume 1 (a,d,g), and Volume 2 GTI = 3°C (b,e,h) and 5°C (c,f,i).

References

Basile, S., A. R. Crimmins, C. W. Avery, B. D. Hamlington, and K. E. Kunkel, 2023. “Appendix 3. Scenarios and Datasets.” *Fifth National Climate Assessment*. Crimmins, A. R., C. W. Avery, D. R. Easterling, K. E. Kunkel, B. C. Stewart, and T. K. Maycock, Eds. U.S. Global Change Research Program, Washington, DC, USA. https://doi.org/10.7930/NCA5.2023.A3

Cheng, L. and A. AghaKouchak, 2014. “Nonstationary Precipitation Intensity-Duration-Frequency Curves for Infrastructure Design in a Changing Climate.” *Scientific Reports,* 4(1), 1-6. https://doi.org/10.1038/srep07093

Daly, C., W. P. Gibson, G.H. Taylor, G.L. Johnson, and P. Pasteris, 2002. “A Knowledge-Based Approach to the Statistical Mapping of Climate.” *Climate Research*, 22(2), 99-113. https://doi.org/10.1002/joc.1688

Daly, C., M. Halbleib, J. I. Smith, W. P. Gibson, M. K. Doggett, G. H. Taylor, J. Curtis, and P. P. Pasteris, 2008. "Physiographically Sensitive Mapping of Climatological Temperature and Precipitation Across the Conterminous United States." *International Journal of Climatology,* 28(15), 2031-2064. https://doi.org/10.1002/joc.1688

Eyring, V., S. Bony, G. A. Meehl, C. A. Stevens, B. Stouffer, R. J. Taylor, and E. Karl, 2016. “Overview of the Coupled Model Intercomparison Project Phase 6 (CMIP6) Experimental Design and Organization.” *Geoscientific Model Development*, 9, 1937-1958, doi:10.5194/gmd-9-1937-2016. https://pcmdi.llnl.gov/CMIP6/

Feitoza Silva, D., S. P. Simonovic, A. Schardong, and J. Avruch Goldenfum, 2021. “Introducing Non-Stationarity into the Development of Intensity-Duration-Frequency Curves Under a Changing Climate.” *Water,* 13(8), 1008. https://doi.org/10.3390/w13081008

Hayhoe, K., A. Stoner, D.J. Wuebbles, and I. Scott-Fleming, 2023. “STAR-ESDM: A Generalizable Approach to Generating High-Resolution Climate Projections through Signal Decomposition.” *Authorea Preprints*.10.22541/essoar.169462036.65393270/v1

Hayhoe, K., I. Scott-Fleming, A. Stoner, and D. J. Wuebbles, 2024. “STAR-ESDM: A generalizable approach to generating high-resolution climate projections through signal decomposition.” *Earth's Future*, 12, e2023EF004107. https://doi.org/10.1029/2023EF004107

Intergovernmental Panel on Climate Change (IPCC), 2023. “Summary for Policymakers.” *Climate Change 2023: Synthesis Report. Contribution of Working Groups I, II and III to the Sixth Assessment Report of the Intergovernmental Panel on Climate Change* [Core Writing Team, H. Lee and J. Romero (eds.)]. IPCC, Geneva, Switzerland, 1-34. 10.59327/IPCC/AR6-9789291691647.001.

Jay, A. K., A. R. Crimmins, C. W. Avery, T. A. Dahl, R. S. Dodder, B. D. Hamlington, A. Lustig, K. Marvel, P. A. Méndez-Lazaro, M. S. Osler, A. Terando, E. S. Weeks, and A. Zycherman, 2023: "Ch. 1. Overview: Understanding Risks, Impacts, and Responses." In: *Fifth National Climate Assessment*. Crimmins, A. R., C. W. Avery, D. R. Easterling, K. E. Kunkel, B. C. Stewart, and T. K. Maycock, Eds. U.S. Global Change Research Program, Washington, DC, USA. https://doi.org/10.7930/NCA5.2023.CH1

Kim, H., S. Kim, H. Shin, and J. H. Heo, 2017. “Appropriate Model Selection Methods for Nonstationary Generalized Extreme Value Models.” *Journal of Hydrology*, 547, 557-574. https://doi.org/10.1016/j.jhydrol.2017.02.005

Lee, J.-Y., J. Marotzke, G. Bala, L. Cao, S. Corti, J. P. Dunne, F. Engelbrecht, E. Fischer, J. C. Fyfe, C. Jones, A. Maycock, J. Mutemi, O. Ndiaye, S. Panickal, and T. Zhou, 2021: "Future Global Climate: Scenario-Based Projections and Near-Term Information." In *Climate Change*

2021: The Physical Science Basis. Contribution of Working Group I to the Sixth Assessment Report of the Intergovernmental Panel on Climate Change [Masson-Delmotte, V., P. Zhai, A. Pirani, S. L. Connors, C. Péan, S. Berger, N. Caud, Y. Chen, L. Goldfarb, M. I. Gomis, M. Huang, K. Leitzell, E. Lonnoy, J. B. R. Matthews, T. K. Maycock, T. Waterfield, O. Yelekçi, R. Yu, and B. Zhou (eds.)]. Cambridge University Press, Cambridge, United Kingdom and New York, NY, USA, pp. 553–672, doi:10.1017/9781009157896.006.

Marvel, K., W. Su, R. Delgado, S. Aarons, A. Chatterjee, M. E. Garcia, Z. Hausfather, K. Hayhoe, D. A. Hence, E. B. Jewett, A. Robel, D. Singh, A. Tripati, and R. S. Vose, 2023. “Ch. 2. Climate trends.” *Fifth National Climate Assessment.* Crimmins, A. R., C. W. Avery, D. R. Easterling, K. E. Kunkel, B. C. Stewart, and T. K. Maycock, Eds. U.S. Global Change Research Program, Washington, DC, USA. https://doi.org/10.7930/NCA5.2023.CH2

Mearns, L., S. McGinnis, D. Korytina, R. Arritt, S. Biner, M. Bukovsky, H. I. Chang, O. Christensen, D. Herzmann, Y. Jiao, and S., Kharin, 2017. “The NA-CORDEX Dataset, Version 1.0.” *NCAR Climate Data Gateway*, Boulder CO. https://doi.org/10.5065/D6SJ1JCH

National Academies of Sciences, Engineering, and Medicine (NASEM), 2024. "Modernizing Probable Maximum Precipitation Estimation." Washington, DC: The National Academies Press. https://doi.org/10.17226/27460.

National Aeronautics and Space Administration (NASA), CGIAR Consortium for Spatial Information (CGIAR-CSI). *SRTM 90m Digital Elevation Data from the CGIAR-CSI Consortium for Spatial Information*. Retrieved on November 30, 2023 from https://cmr.earthdata.nasa.gov/search/concepts/C1214622194-SCIOPS.

National Centers for Environmental Information (NCEI), NOAA. *Climate at a Glance: Global Time Series*. Published November 2023, retrieved on November 30, 2023 from https://www.ncei.noaa.gov/access/monitoring/climate-at-a-glance/global/time-series.

Neelin, J. D., C. Martinez-Villalobos, S. N. Stechmann, F. Ahmed, G. Chen, J. M. Norris, Y. H. Kuo, and G. Lenderink, 2022. "Precipitation Extremes and Water Vapor: Relationships in Current Climate and Implications for Climate Change." *Current Climate Change Reports*, 8(1), 17-33. https://doi.org/10.1007/s40641-021-00177-z.

Office of Water Prediction (OWP), National Weather Service, 2022. *Analysis of Impact of Nonstationary Climate on NOAA Atlas 14 Estimates Assessment Report*. https://hdsc.nws.noaa.gov/pub/hdsc/data/papers/NA14_Assessment_report_202201v1.pdf.

O’Gorman, P.A., 2015. "Precipitation Extremes Under Climate Change." *Current Climate Change Reports*, 1, 49-59. https://doi.org/10.1007/s40641-015-0009-3

O’Neill, B. C., E. Kriegler, K. L. Ebi, E. Kemp-Benedict, K. Riahi, D. S. Rothman, B. J. van Ruijven, D. P. van Vuuren, J. Birkmann, K. Kok, M. Levy, and W. Solecki, 2017. "The Roads Ahead: Narratives for Shared Socioeconomic Pathways Describing World Futures in the 21st Century." *Global Environmental Change*. https://doi.org/10.1016/j.gloenvcha.2015.01.004.

Panagoulia, D., P. Economou, and C. Caroni, 2014. “Stationary and Nonstationary Generalized Extreme Value Modelling of Extreme Precipitation Over a Mountainous Area Under Climate Change.” *Environmetrics, 25(1)*, 29-43. https://doi.org/10.1002/env.2252

Perica, S., S. Pavlovic, M. St. Laurent, C. Trypaluk, D. Unruh, and O. Wilhite, 2018*. NOAA Atlas 14 Volume 11 Version 2, Precipitation-Frequency Atlas of the United States, Texas.* NOAA, NWS, Silver Spring, MD. https://www.weather.gov/media/owp/oh/hdsc/docs/Atlas14_Volume11.pdf

Pierce, D. W., D. R. Cayan, D. R. Feldman, and M. D. Risser, 2023. “Future Increases in North American Extreme Precipitation in CMIP6 Downscaled with LOCA.” *Journal of Hydrometeorology, 24(5)*, 951-975. 10.1175/JHM-D-22-0194.1

Pierce, D. W., D. R. Cayan, B. L. Thrasher, 2014. “Statistical Downscaling Using Localized Constructed Analogs (LOCA).” *Journal of Hydrometeorology, 15(6),* 2558-2585. http://dx.doi.org/10.1175/JHM-D-14-0082.s1

Seneviratne, S.I., X. Zhang, M. Adnan, W. Badi, C. Dereczynski, A. Di Luca, S. Ghosh, I. Iskandar, J. Kossin, S. Lewis, F. Otto, I. Pinto, M. Satoh, S.M. Vicente-Serrano, M. Wehner, and B. Zhou, 2021. "Weather and Climate Extreme Events in a Changing Climate." In *Climate Change 2021: The Physical Science Basis. Contribution of Working Group I to the Sixth Assessment Report of the Intergovernmental Panel on Climate Change.* [Masson-Delmotte, V., P. Zhai, A. Pirani, S.L. Connors, C. Péan, S. Berger, N. Caud, Y. Chen, L. Goldfarb, M.I. Gomis, M. Huang, K. Leitzell, E. Lonnoy, J.B.R. Matthews, T.K. Maycock, T. Waterfield, O. Yelekçi, R. Yu, and B. Zhou, Eds.] Cambridge University Press, Cambridge, United Kingdom and New York, NY, USA, pp. 1513–1766. https://doi.org/10.1017/9781009157896.013.

United States Global Change Research Program (USGCRP), 2023*. Fifth National Climate Assessment.* Crimmins, A. R., C. W. Avery, D. R. Easterling, K. E. Kunkel, B. C. Stewart, and T. K. Maycock, Eds. U.S. Global Change Research Program, Washington, DC, USA. https://doi.org/10.7930/NCA5.2023

Vu, T. M. and A. K. Mishra, 2019. “Nonstationary Frequency Analysis of the Recent Extreme Precipitation Events in the United States.” *Journal of Hydrology, 575*, 999-1010. https://doi.org/10.1016/j.jhydrol.2019.05.090

Appendix A: Acronyms and Abbreviations

AEP	Annual Exceedance Probability
AIC	Akaike Information Criterion
AICc	Corrected Akaike Information Criterion
AMS	Annual Maximum Series
CMIP5	Coupled Model Intercomparison Project Phase 5
CMIP6	Coupled Model Intercomparison Project Phase 6
DDF	Depth-duration-frequency
DEM	Digital Elevation Model
GCM	General Circulation Model
GEV	Generalized Extreme Value
GTI	Global Temperature Index
IPCC	Intergovernmental Panel on Climate Change
LOCA2	Localized Constructed Analogs Version 2
MAM	Mean Annual Maximum
MAP	Mean Annual Precipitation
MLE	Maximum Likelihood Estimation
NA-CORDEX	North American Coordinated Regional Downscaling Experiment
NCA5	Fifth National Climate Assessment
NCEI	National Centers for Environmental Information
NOAA	National Oceanic and Atmospheric Administration
NWS	National Weather Service
OWP	Office of Water Prediction
PF	Precipitation Frequency
PRISM	Parameter-Elevation Regressions on Independent Slopes Model
SRTM90	90-meter Shuttle Radar Topographic Mission
SSP	Shared Socioeconomic Pathway
STAR-ESDM	Seasonal Trends and Analysis of Residuals Empirical-Statistical Downscaling Model

Appendix B: Glossary

Adjustment Factor – A multiplicative term that is applied to Atlas 15 Volume 1 precipitation frequency estimates to obtain future estimates for Volume 2. Adjustment factors are computed based on an analysis of GCM datasets.

Annual Exceedance Probability (AEP) - The probability associated with exceeding some precipitation depth for a specified duration at least once for any given year. The inverse of AEP provides a measure of the average time between years (not events) in which a particular value is exceeded at least once. The term is associated with analysis of annual maximum series.

Annual Maximum Series (AMS) – A time series of the largest precipitation amounts in a continuous 12-month period (calendar or water year) for a specified duration at a given location.

Constrained Precipitation – Total precipitation depth during a fixed window of time that often corresponds with observer records (e.g., 8:00 am – 8:00 am for 1-day totals). This observation requires conversion to an unconstrained value (see **Unconstrained Precipitation**) because the maximum time-integrated precipitation totals rarely fall within the constrained window of time.

Depth-Duration-Frequency (DDF) Curve – Graphical depiction of precipitation frequency estimates in terms of depth, duration and frequency (AEP for AMS).

General Circulation Model (GCM) – Dynamical numerical model used to represent physical processes within Earth's climate system. Global CGMs typically have relatively coarse spatial resolutions (50 - 250 km) and can be run over past time periods or future time periods, resulting in hindcast or forecast simulations, respectively.

Generalized Extreme Value (GEV) Distribution – A family of continuous probability distribution functions that can be used to describe the behavior of extreme events. The distribution is defined by three parameters: location, scale, and shape.

Global Temperature Index (GTI) – Annual, or multi-year averaged, global-average temperature anomaly, relative to preindustrial values. For Atlas 15 Volume 1, GTI is defined as the 30-year averaged global temperature anomaly based on observation, and for Atlas 15 Volume 2, GTI is defined by anomalies averaged across multiple GCMs.

Mean Annual Maximum (MAM) - The average of annual maximum series data for a specified duration and location.

Mean Annual Precipitation (MAP) – The average precipitation for a year (usually calendar). Can be based on the whole period of record or for a selected period (usually 30-year period such as 1971-2000).

Maximum Likelihood Estimation (MLE) – Method of estimating distribution parameters by optimization of the log-likelihood function to ensure the optimal fit to a given sample.

Precipitation Frequency (PF) – For the AMS-based analysis, annual exceedance probability associated with specific precipitation magnitude for a given duration and location.

Shared Socioeconomic Pathway (SSP) – Climate change scenarios that describe changes in global radiative forcing based on socioeconomic projections through 2100.

Unconstrained precipitation – Total precipitation depth during a moving window of time that encompasses the maximum depth for a specified duration.

See also https://www.weather.gov/owp/hdsc_glossary for more standard definitions.